Universität Rostock

Traditio et Innovatio

Laser-driven electron and spin-state quantum dynamics in transition metal complexes

Kumulative Dissertation

zur Erlangung des akademischen Grades
doctor rerum naturalium (Dr. rer. nat.)
der Mathematisch-Naturwissenschaftlichen Fakultät
der Universität Rostock

Rostock, 2018

vorgelegt von:
Huihui Wang
aus China, Shanxi
geboren am 02. Februar 1989 in Shanxi

urn:nbn:de:gbv:28-diss2018-0166-0

Promotion

Mathematisch-Naturwissenschaftliche Fakultät

Gutachter:

1. Gutachter:

   Prof. Dr. Oriol Vendrell

   Physikalisch-Chemisches Institut, Universität Heidelberg

2. Gutachter:

   Prof. Dr. Oliver Kühn

   Institut für Physik, Universität Rostock

3. Gutachter:

   Dr. Sergey Bokarev

   Institut für Physik, Universität Rostock

Datum der Einreichung: 24. Juli 2018

Datum der Verteidigung: 09. November 2018

Abstract

Recent advances in attosecond spectroscopy open the door to understanding more and more intricate effects on the atomic scale, such as, the correlated motion of valence and core electrons. For valence excitations, processes related to the electron spin are usually driven by nuclear motion. However, when going to the core-excited states where the core hole has a nonzero angular momentum, the strong spin-orbit coupling starts to play the dominating role.

In this thesis, a theoretical method called density matrix-based time-dependent restricted active space configuration interaction is developed to study the non-equilibrium electron and spin dynamics of transition metal complexes. Compared to other methods suggested before, this method accounts for the interplay of electron correlation and spin-orbit coupling. The spin-orbit coupling between electronic states of different multiplicity is considered within the LS-coupling limit employing the atomic mean-field integral approximation.

Using this method, we theoretically addressed the unprecedentedly ultrafast spin-flip dynamics for L-edge ($2p \rightarrow 3d$) excited states of a prototypical $[Fe(H_2O)_6]^{2+}$complex. The timescale of such processes is faster than the core-hole lifetime (about 4 fs). Ultrashort pulses can be used as practical means to prepare complex superpositions of quantum states and then to manipulate and steer their dynamics. In this thesis, we also simulate the spin-flip dynamics which is initiated by isolated sub-fs soft X-ray pulses and X-ray pulse trains, trying to approximately model the possible X-ray free electron laser and high harmonic generation setups. Interestingly, modest variations of carrier frequency, amplitude, and pulse duration can lead to substantial changes in the spin-state composition, suggesting its control by soft X-ray light. Besides, we also take into account energy dissipation and coherence dephasing caused by the nuclear vibrations, treated at the level of system-bath partitioning.

In conclusion, the timescale of the electron dynamics driven by the spin-orbit coupling suggests using it for clocking ultrafast events. The detailed study presents a novel perspective and helps to gain a fundamental understanding of spin crossover processes, which can be accessed by attosecond experiments. We expect the experimental verification of the ultrafast electronic spin-flip process and believe that manipulating spin dynamics by X-ray laser light appears to be within reach.

Zusammenfassung

Jüngste Fortschritte in der Attosekundenspektroskopie öffnen die Tür zum Verständnis komplizierter Effekte auf der atomaren Skala, wie beispielsweise, der korrelierten Bewegung von Valenz- und Kernelektronen. Bei Valenzanregungen werden Prozesse, die mit dem Elektronenspin in Zusammenhang stehen, gewöhnlich erst durch die Kernbewegung ermöglicht. Wenn man jedoch zu innerschalenangeregten Zuständen geht, in denen das Innerschalenloch einen von Null verschiedenen Drehimpuls hat, beginnt die starke Spin-Bahn-Kopplung die dominierende Rolle zu spielen.

In dieser Arbeit wurde eine theoretische Methode entwickelt, die auf einer dichtematrixbasierten, zeitabhängigen Konfigurations-Wechselwirkungsmethode mit eingeschränkten aktiven Räumen beruht, um die Elektron-Spin-Nichtgleichgewichtsdynamik von Übergangsmetallkomplexen zu untersuchen. Im Vergleich zu anderen Methoden, die zuvor vorgeschlagen wurden, berücksichtigt diese Methode das Zusammenspiel von Elektronenkorrelation und Spin-Bahn-Kopplung. Die Spin-Bahn-Kopplung zwischen elektronischen Zuständen unterschiedlicher Multiplizität wird innerhalb des Grenzfalls der LS-Kopplung berücksichtigt, wobei die Integrale mittels der Methode der atomar gemittelten Felder approximiert werden.

Mittels dieser Methode haben wir die beispiellose ultraschnelle Spin-Flip-Dynamik für angeregte L-Kanten- ($2p \rightarrow 3d$) -Zustände eines prototypischen $[Fe(H_2O)_6]^{2+}$Komplexes theoretisch beschrieben. Die Zeitskala eines solchen Prozesses ist schneller als die Lebensdauer der Innerschalenlochs (etwa 4 fs). Ultrakurze Pulse können verwendet werden, um komplexe Superpositionen von Quantenzuständen zu erzeugen und ihre Dynamik zu manipulieren und zu steuern. In dieser Arbeit simulieren wir weiterhin auch die Spin-Flip-Dynamik, die durch isolierte Sub-fs Röntgenpulse und Röntgenpulszüge angeregt wird und versuchen dabei, mögliche Setups des Röntgen-Freie-Elektronen-Lasers und der Erzeugung hoher Harmonischer annähernd zu modellieren. Interessanterweise können moderate Variationen der Trägerfrequenz, der Amplitude und der Pulsdauer zu substanziellen Änderungen der Spinzustandsverteilung führen, was auf eine Kontrolle durch weiches Röntgenlicht schließen lässt. Außerdem berücksichtigen wir die Energiedissipation und die Kohärenzdephasierung, die durch die Kernvibrationen verursacht werden, und zwar auf dem Niveau eines System-Bad-Modells.

Schlussfolgernd lässt sich sagen, dass die Zeitskala der Elektronendynamik, die durch die Spin-Bahn-Kopplung gesteuert wird, für die Messung ultraschneller Ereignisse genutzt werden kann. Die vorliegende detaillierte Studie bietet eine neue Perspektive und hilft, ein grundlegendes Verständnis von Spin-Crossover-Prozessen zu erhalten, die durch Attosekunden-Experimente zugänglich sind. Wir erwarten die experimentelle Verifikation des ultraschnellen elektronischen Spin-Flip-Prozesses und glauben, dass die Manipulation der Spindynamik durch Röntgenlaserlicht

in Reichweite ist.

List of Abbreviations

ρ-TD-RASCI	density matrix-based time-dependent restricted active space configuration interaction
ADC	algebraic diagrammatic construction
AMFI	atomic mean-field integral
CI	configuration interaction
CM	charge migration
CSF	configuration state function
EUV	extreme ultraviolet
FWHM	full width at half maximum
HF	Hartree-Fock
HHG	high harmonic generation
IR	infrared
MCSCF	multi-configurational self-consistent-field method
MO	molecular orbital
PES	potential energy surface
RASSCF	restricted active space self-consistent-field
SCO	spin crossover
SD	slater determinant
SF	spin free
SOC	spin-orbit coupling
SRIXS	stimulated resonant inelastic X-ray scattering
TD-CI	time-dependent configuration interaction
TD-SCF	time-dependent self-consistent-field
TM	transition metal
XFEL	X-ray free-electron laser

On the convention

At the beginning of the thesis, I will firstly introduce conventions for symbols and quantities used throughout this work: $\hat{O}$ – operators, $\mathcal{A}$ – superoperators, $\vec{a}$ – vectors, $\mathbf{A}$ – matrices. In most cases, atomic units (a.u.) will be used ($m_e = 1$, $\hbar = 1$) in Methodology chapter to write working expressions in a compact form. In the Results and Discussion chapter, mostly eV and fs (femtosecond) are used as energy and time units, thus the $\hbar$ factor is retained.

Contents

I Introduction **1**
1 From Femtosecond to Attosecond Physics . . . 1
2 X-ray Free Electron Lasers . . . 2
3 High Harmonic Generation . . . 3
4 Applications of Ultrashort Pulses . . . 5
5 Charge Migration after Ionization or Excitation . . . 6
6 Spin Crossover . . . 8

II Developed Theoretical Methodology **11**
1 System-Bath Partitioning . . . 11
2 Choice of the Basis . . . 12
3 Electronic Structure Method . . . 13
4 Light-Matter Interaction . . . 14
5 Dissipative Dynamics . . . 15

III Results and Discussion **17**
1 Model System . . . 17
2 Considered Dynamic Regimes . . . 18
3 Electron Correlation-driven Dynamics . . . 19
4 Spin-Orbit Coupling-driven Dynamics . . . 19
5 Explicit Field Excitation . . . 22
5.1 Single Pulse . . . 22
5.2 Pulse Trains . . . 23
6 Energy Dissipation . . . 26

IV Conclusions and Outlook **28**

A Own Contributions to the Manuscripts **45**

B Peer Reviewed Publications **46**
[**HW1**] Published in the *Physical Review Letters* **118**, 023001 (2017) . . . 46
[**HW2**] Published in the *Molecular Physics* **115**, 1898-1907 (2017) . . . 47
[**HW3**] Published in the *Physical Review A* **98**, 013408 (2018) . . . 48

Chapter I

Introduction

1 From Femtosecond to Attosecond Physics

Molecules contain electrons and nuclei whose dynamics takes place on a multitude of timescales, ranging from attoseconds for electrons to picoseconds or longer for vibrations or conformational changes. These dynamics are very intricate because the complex many-body character of interaction of electrons between themselves as well as with nuclei. In general, the properties of matter are ultimately determined by the electronic structure, so understanding its details is a crucial step to design the properties of a molecular system. The multi-electron problem has already attracted much attention, for instance in theoretical investigations [1, 2, 3, 4]. Even though it has been studied for about a century, the understanding of the dynamics of electrons on the atomic scale still remains a challenge. That is because in the atomic system, the timescale of the electron movement, especially for core electrons, exceeds the time resolution limit of any detection technique. So the exploration or direct measurement of such motion has driven scientists's enthusiasm to find a tool on the same or shorter time scales. This has inspired the technological revolution in twentieth century that contain the development of lasers and non-linear spectroscopic techniques.

The discovery of the laser offered a new possibility to trigger, control and manipulate atomic and molecular processes, such as, rotational, vibrational and electronic excitations [5, 6, 7]. Fig. I.1 shows the corresponding characteristic length- and timescales for different structures and dynamics relevant for molecular and atomic physics. The typical timescale for these processes range from hundreds of picoseconds ($1\,\mathrm{ps} = 10^{-12}\,\mathrm{s}$) for molecular rotations down to few attosecond ($1\,\mathrm{as} = 10^{-18}\,\mathrm{s}$) for electronic motion. To observe these fast processes, one requires short laser pulses. Rapid technological processes especially the invention of laser locking technology [8], promoted generation of shorter and shorter laser pulses. In 20th century, along with the advent of femtosecond laser, the pump-probe techniques allowed to trace the changes in the ultrafast chemical reaction processes such as the breaking and formation of the chemical bonds or the vibrations in molecules [9, 10, 11]. Zewail's pioneering 1987 experiment [12] has been widely recognized and resulted in the award of a Nobel Prize in 1999, which led to the birth of a new research area–femtochemistry. Since then femtosecond spectroscopy has been intensively applied to study processes in gases [13], fluids [14], solids [15, 16], on surfaces [17, 18, 19], and in polymers [20, 21]. This research not only explicated how to design catalysts [22, 23] and

molecular electronic components [21] but also addressed the most delicate mechanisms of life processes such as photosynthesis. Moreover, it guided scientists how to synthesize useful organic molecules as fuels [24] and produce medicines of the future [25].

However, to resolve the electronic dynamical processes in time domain, a laser pulse must be much shorter than femtosecond. With the rapid development of ultrafast science, researchers were able to compress the infrared femtosecond pulse to near one optical cycle (2.4-4 fs) [26, 27]. Nonetheless, to further reduce the pulse duration to less than one femtosecond by traditional optical pulse compression method, requires its full width at half maximum (FWHM) to be increased above 2 eV, what is a technological challenge.

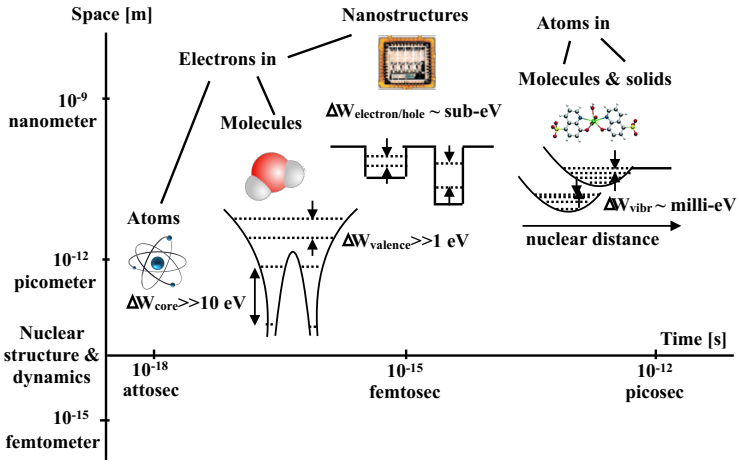

Figure I.1: Characteristic length- and time-scales for structures and processes relevant to molecular and atomic physics. Reprinted with permission from F. Krausz and M. Ivanov, Reviews of Modern Physics, 81, 163-234, (2009). Copyright 2009 by the American Physical Society.

In principle, it is more feasible to generate attosecond pulses in the extreme ultraviolet (EUV) or soft X-ray ranges. So far, a variety of methods have been proposed, such as stimulated Raman scattering [28, 29], plasma mirror generation [30, 31], X-ray free-electron lasers (XFELs) [32, 33] and high harmonic generation (HHG) [34]. Stimulated Raman scattering, although having a solid theoretical background, lacks the proper medium what limits the bandwidth of the pulses. So far such method was implemented only to produce few femtosecond pulses in EUV range [35]. Plasma mirror technique utilizing the relativistic nonlinearity of plasma to obtain EUV radiation has been proposed in theory, but no relevant experiment has been yet reported. Thus, to date XFELs and high harmonic generation (HHG) are the two main experimental techniques to generate the high-energy ultrashort pulses. XFELs are designed to produce isolated light pulse while HHG typically generates the trains of such pulses. However, with additional effort and loss of intensity one can also generate isolated pulses using HHG. These two setups are the most important in the context of this work. The dynamics initiated by isolated pulses is considered in Publications [**HW1,2**], thus resembling a possible XFEL experiment. The effect of HHG trains of pulses is discussed in Publication [**HW3**]. Both cases are described in Chapter III below.

2 X-ray Free Electron Lasers

X-ray spectroscopy is a unique and widely used element-specific method for determining the electronic and local geometric structure of matter. X-rays can be emitted or absorbed during inner-shell electronic transitions. X-rays access the core-excited states and ionized states and have characteristic energies related to the atomic number. This means that each element has a

characteristic X-ray spectrum.

XFELs have been designed for generating high brightness coherent ultrashort pulses in the vacuum and extreme ultraviolet or X-ray energy region [36, 37], outperforming by far accelerator-based synchrotron sources. XFELs are based on the Bremsstrahlung principle and use free electrons as a gain medium to amplify the electromagnetic radiation. The beam of the electrons can be accelerated to almost the speed of light passing through periodically alternating magnets (called undulators).The accelerated electrons fly along a sinusoidal path along the axis of the undulators what results in the emission of electromagnetic radiation. Due to the same period of the electron oscillations and the emitted radiation, the waves emitted by individual electrons are added constructively. The total emission intensity of all electrons has an exponential increase with the distance, travelled along the undulator. Since mirrors are ineffective for X-rays, there is no possibility to build an optical cavity. Hence, XFELs are designed with a long undulator to gain high intensity and ultimately reach the saturation. Control of the energy of electron beam as well as period and strength of the undulator enables one to tune the wavelength of the emitted radiation.

Generally, the intensity of X-ray pulses produced by XFELs is much higher than that of conventional synchrotron light sources (average brilliance is 10000 times higher, peak brilliance is a billion times higher) [38]. However, the typical ultraintense X-ray pulses are from few to hundred femtoseconds long, and thus can not be used to investigate ultrafast electron dynamics on the atomic or molecular scale. Until now, various schemes have been proposed to generate intense attosecond pulses by XFELs [32, 39, 40, 41]. The critical point of these techniques to reduce the duration of the pulse is manipulation of the electrons, allowing only a short section of the electron wave to emit. Another method called X-ray Laser-Enhanced Attosecond Pulse generation (XLEAP) is currently developed at the SLAC National Accelerator Laboratory, and is expected to produce coherent intense pulses which can be narrowed down to only few hundred attoseconds [42]. Although XFEL facilities are close to creating attosecond pulses, but it is hard to prove and characterise the existence of such short pulse. Only after direct measurement of the time and energy structure of short X-ray pulses, one can say that the real time-resolved experiment is upcoming. For instance, a method called angular streaking has been proposed to characterise the time and energy structure of XFEL pulses [43]. Even though, currently, there are no XFEL facilities which could generate the suitable attosecond X-ray pulse for pump-probe experiments with various time delays below femtosecond regime, we expect it to be available in the future.

X-ray FELs give us an unprecedented view of the structure and dynamics of matter at the small length- (about one Angstrom) and small time scale (few femtoseconds). So far, it has been used in various fields based on its wide frequency range, such as, high energy, atomic, plasma, condensed matter physics, chemistry, biology, medicine and military applications [38, 44, 45].

3 High Harmonic Generation

In nonlinear optics, light with high intensity propagating in a medium can produce new frequency components [46]. For example, an atom can absorb more than two photons, then a high energy photon is emitted, thus generating high-order harmonics. Currently, HHG provides an effective

way to produce attosecond pulses in the experiment. Higher harmonics are essentially a result of coherent electron-ion collisions induced by strong fields. The physical picture can be well explained by a semiclassical three-step model [47]. In HHG, the intense femtosecond laser pulse is focused into a gas jet, mostly noble gas. The electric field of the intense laser pulse must be comparable or stronger than the atomic Coulomb potential, such that tunnelling process can take place. Firstly, the electric field of the laser pulse distorts and bends the electronic potential and allows the electronic wave packet to leave the vicinity of the nucleus via tunnelling through the potential barrier. Then this electronic wave packet is accelerated and gains kinetic energy in the electric field as a free electron. After that, because the force exerted by electromagnetic radiation is reversed, the electron decelerates, changes its direction of the motion and moves back towards its original position. Recolliding and recombining with its parent ion is accompanied by release of the excess kinetic energy in form of a high-energy photon.

Most HHG photons have been limited to the EUV region with the energy less than 150 eV [34, 48]. Nevertheless, scientists demand the pulse extending to the soft X-ray region (150 eV to 5 keV) to directly study the electronic and spin dynamics in the molecules. From the three step model, the highest emitted photon energy follows the cut-off law: $h\nu_{\text{cutoff}} = I_p + 3.17U_p$, where h is Planck's constant, ν is the frequency, U_p and I_p are ponderomotive energy and ionisation energy, respectively. Obviously, according to this equation, the cutoff energy can be significantly increased in two ways: using a higher intensity of the driving laser or using the long wavelength electric field [49, 50, 51, 52]. However, both of these two ways suppresses the conversion efficiencies of HHG. Therefore, considering the competition of cut-off energy and conversion efficiency, ultrashort infrared (IR) pulses with wavelength of 1.5-3 μm are regarded as the most suitable driving pulses to generate attosecond pulses reaching X-ray region. It has been reported that using midinfrared femtosecond driving lasers in a gas, enables generation of bright, coherent X-ray supercontinua with photon energy up to 1.6 keV [53]. Meanwhile, the low conversion efficiency, especially for IR driven HHG in soft X-ray region, limits the applications in science and technology. It has been proposed that modification of the driving waveform can increase the conversion efficiency of HHG, i.e. by controlling the ionization and acceleration of the free electron by reshaping the driving electric field. Recently, an enhancement approach named two-color-driven HHG has been discussed both in theory and experiment [54, 55]. It uses fundamental and its third harmonic (ω + 3ω) as the "control" field, the efficiency enhancement reaches up to factor of eight for lower photon energy compared to the single-color-driven cases [56]. The authors expect that such approach could be further useful towards higher efficiency enhancement in soft X-ray range finding a global optimum condition. Besides, the choice of the medium is also important for the enhancement of HHG.

In HHG, tunnelling ionization takes place and can create an attosecond pulse within half cycle of the laser field. This means that multi-cycle driving pulse typically generates an attosecond pulse train separated by half cycle of the driving pulse field, since ionization, acceleration and recombination processes are repeated every half cycle of the driving laser field. However, the short interpulse spacing of the train of attosecond pulses limits its use in pump-probe experiment as it launches replicas of electronic wave packets which interfere with each other. Therefore, isolated attosecond pulses are required. Besides XFELs, it is also possible to generate isolated

pulses with HHG but this requires an additional complexity of the setup [57]. The corresponding trick is to use a gating to confine the harmonic radiation to a single emission event, such as amplitude gating technique [58], double optical gating [59, 60], polarization gating [61, 62], ionization gating [63, 64], as well as the recent techniques named attosecond lighthouse [65] and noncollinear optical gating [66]. Within these methods, the duration of the isolated pulses generated by HHG has been reduced to 53 as [67], which is new record up to now, and is approaching the atomic unit of time (24 as). However, the generated isolated pulse has a much lower intensity than the pulse train, which is not strong enough to be employed in pump-probe experiment. We expect and believe that the intense isolated pulse can be generated by HHG in the future. In my work, not only isolated pulses (more typical for XFELs) but also trains of pulses (typical for HHG) are studied, more detailed discussion can be found in Section III. 5.

4 Applications of Ultrashort Pulses

Since isolated single attosecond pulses have been generated from HHG and XFELs, a new chapter in ultrafast spectroscopy was opened. Recently, the few-cycle optical pulses in the near-IR, visible and near-ultraviolet spectral regions with duration shorter than 10 fs have been used to develop such spectroscopic techniques as impulsive vibrational [68, 69], time-resolved stimulated Raman [70, 71], and ultrafast pump-probe absorption spectroscopy [72, 73].

The pump-probe experiments have made a major impact on the understanding of light-matter interaction [49, 74, 75, 76]. To date, measurements with attosecond temporal resolution have been performed by using an isolated attosecond pulse as pump and subsequent IR femtosecond pulse as a probe after some adjustable time delay, or vice versa. Experiments using isolated attosecond pulses both as pump pulse to initiate system dynamics and as probe pulse to monitor it could be a real breakthrough. However, until now, they have not been possible, even though some experiments have come very close [72]. The extremely low pulse intensity of the available attosecond sources (below 10^{14} W/cm^{-2}) is the main reason and the crucial limitation that prevented the demonstration of attosecond-pump/attosecond-probe scheme [77].

The femtosecond time-resolved spectroscopy has been used to investigate the photoexcitation and photoionization [78, 79], to explore the electronic dynamics in molecules like electron redistribution and localisation [80], or to study spin crossover (SCO) or spin-flip in some metal complexes [81, 82, 83], to name several examples. When exposing molecules to the light pulses of sub-fs duration, electronic wave packets which comprise many electronic eigenstates can be created, and subsequently evolve in time. Therefore, applying the ultrashort pulses to a molecule can trigger electron dynamics, probe the electron "trajectory" and the response due to the interaction between light and matter [73, 84]. Further, it gives access to, for example, electron correlation manifesting itself in the entanglement of bound- and photo-electrons (shake-ups), Auger and interatomic Coulomb decay, charge migration as well as to the coupling of electrons in plasmonic systems [80, 85, 86, 87]. In next two sections, I will shortly review two processes which are related to the main topic of the present dissertation: charge migration (CM) and spin crossover (SCO).

Further, X-ray pulses can also directly access the coherent dynamics of valence or inner-shell electrons with unprecedented temporal resolution. The higher-energy soft X-ray pulses which

simultaneously cover several absorption edges in combination with attosecond time resolution now have drawn much attention [88]. Using the ultrashort X-ray light can capture and monitor the dynamics of charges, spins, atoms, and phonons through the transient X-ray absorption spectroscopy as the state or shape of material or molecular geometry changes [89, 90, 91]. Moreover, catalytic materials (e.g. containing Fe, Co, Ni, Cu), whose inner-shell absorption edges lie at photon energies close to 1 keV [92, 93], can also be analyzed. In my work, the isolated as well as trains of soft X-ray pulses are used to study the electronic dynamics theoretically. In publications [**HW1,2**], we only study the ultrafast spin dynamics triggered by the isolated soft X-ray pulses, modelling the XFELs setup, the detailed results are discussed in Section III. 5.1. In the publication [**HW3**], we consider the effects of the trains of soft X-ray pulses on spin dynamics, modelling HHG, as discussed in Section III. 5.2.

5 Charge Migration after Ionization or Excitation

Charge migration (CM) is a prominent example of ultrafast electron dynamics arising whenever many electronic states are forming a wave packet. Charge migration (CM) takes place following the ionization or excitation of the system [94, 95, 96]. Upon ionization with ultrashort pulses, an electron is removed suddenly from the ground state of the system creating a hole in the electron cloud. If the bandwidth of the ionizing pulse is large enough, this process corresponds to preparation of a non-stationary coherent superposition of eigenstates which evolves in time. In principle, the intense ultrashort pulses permit removing the electron from different orbitals of the system in a controlled way, steering and manipulating the motion of electrons in real time [57]. In recent years, it is advocated that tuning the carrier frequency of a broadband X-ray pulses is an accessible method to create wave packets of the valence electrons and holes localized in the selected atom [97].

The hole will be filled by neighbouring electrons, creating another hole again, and thus, as the time proceeds, the hole migrates throughout the molecules (Fig. I.2). When the excitation of the system is considered, both the hole and the excited electron (particle) may migrate.

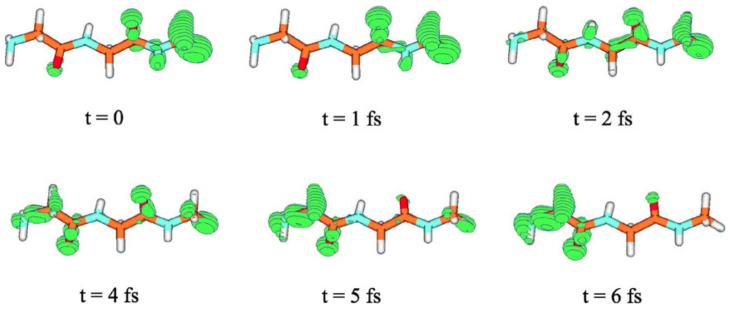

Figure I.2: Snapshots of the evolution of the hole density after ionization from inner-valence orbital of the C_s symmetric conformer of Gly-Gly-NH-CH_3. Reprinted with permission from Elsevier: A. I. Kuleff, S. Lünnemann, and L. S. Cederbaum, Electron-correlation-driven charge migration in oligopeptides, Chemical Physics, 414, 100-105, (2012). Copyright 2012 Elsevier B.V. All rights reserved.

CM is driven solely by electron correlation. The response of the molecule on the removal of an electron depends on the strength of electron correlation and the molecular orbitals (MOs) relevant for ionization [98]. It is found that CM is much easier observed after ionization in the inner-valence shell than the outer-valence shell. This is because the electron correlation effects in outer-valence shell are typically much weaker than in

the inner-valence shell. After ionization or excitation, CM occurs oscillatory, the hole bounces back and forth between the two site of the molecule on the ultrafast timescale. The period of such ultrafast process can reach few femtoseconds or even attosecond scale [99, 100, 101]. Fig. I.2 shows the snapshots of the evolution of the hole density after inner-valence ionization of oligopeptides. It can be seen that the charge almost completely migrates from the left site to the other side of the molecule within 6 fs. Such studies are important for microscopic understanding of ultrafast transfer phenomena, for example, to approach the fundamental limits of the transmission speed of signals relevant for molecular electronics.

In the last few decades, the ultrafast charge (hole) migration after ionization has attracted attention both from the theoretical [99, 100, 101, 102, 103, 104, 105, 106] and experimental [107, 108] sides, for systems ranging from simple molecules to complex bio-substances. These typical systems contain heavier atoms, like transition metal (TM) complexes [109] or π-electron systems [110, 111], which have low-energy virtual orbitals. In recent years, attosecond pulses have been applied to directly detect the CM of molecules, not only in simple molecules like H_2 or N_2 [112, 113, 114] but also some complex systems [107, 108] in experiment. Moreover, CM after excitation also has been studied, the following quantum dynamics of the particle and hole after excitation has been revealed by simulated time-resolved pump-probe spectroscopy [115] or attosecond X-ray Raman scattering [116].

So far, the two most general and frequently applied theoretical methods to study dynamics for electronic excited states are developed. They are the time-dependent configuration interaction (TD-CI) [4, 117, 118, 119] and time-dependent self-consistent-field (TD-SCF) [119] methods. Within this methods, the wave function is expanded as a linear combination of the slater determinants (SDs) or configuration state functions (CSFs). The corresponding configuration interaction (CI) expansion coefficients are set to be time dependent. For practical reasons, the wave function expansions include only single to at most double excited configurations to save computational time, see Table I.1. Another approach, the algebraic diagrammatic construction (ADC) [120, 121, 122], also provides a way to follow the behavior of the particle-hole system in time after an initial excitation. The ADC scheme of the polarization propagator is derived from many-body Green's function theory and is based on perturbation theory. Within this method, both the ground-state electron correlation and relaxations of surrounding electrons make the contribution to an excited charge distribution. In my work, another CI-like method has been developed to describe the electronic structure of the system, see more details in Chapter II or in publication [**HW2**].

References	**Objects**	**Methods**	**Type**	**Char. time**
Li et al. [123]	Glycine	TD-CI	2h	6 fs
Kuleff et al. [124]	Benzene	ADC	2h1p	1 fs
Nisoli et al. [107]	Phenylalanine	TD-SCF	1h	4.5 fs
Averbukh et al. [125]	Glycine	ADC	2h1p	15 fs
Cederbaum et al. [105]	MePeNNA	ADC	2h1p	7.5 fs

Table I.1: List of theoretical studies of CM in different systems. 1h, 2h, 2h1p correspond to the excitation level, representing one hole, two hole, and two hole one particle configurations, respectively.

Table. I.1 lists some studies of CM for different molecules performed recently. Most of these studies focus on the K-edge hole or valence hole of the molecules and describe the different type of dynamics only accounting for the electron correlation, without taking spin-orbit coupling (SOC) into account. The characteristic time is in the few femtosecond range demonstrating that CM after ionization is really an ultrafast process. In my work, the simulation similar in spirit has been done for TM complex [**HW1-3**], see Chapter II, involving up to 4h4p electronic configurations and taking SOC effects into account.

So far, CM has been considered as a purely electronic process. In this case, Born-Oppenheimer approximation is assumed. Thus, the electron motion is disentangled from the nuclear motion. However, there's no doubt that after a sufficiently long time, the nuclear dynamics will play a role in such processes. This is illustrated by comparing with the cases when nuclei are fixed and allowed to move [126]. After a few femtoseconds the effect of nuclear motion can not be neglected anymore as the energy difference between the mixed states changes with nuclear motion and the coherence is lost. Besides, it is also further elucidated that the CM is extremely sensitive to the geometry of the nuclei [127, 126]. Moreover, some researches have demonstrated that the ultrafast charge transfer driven exclusively by nuclear dynamics can also occurs in few femtoseconds [123]. This finding go against the common wisdom. On the other hand, it was shown that after ionization an electron from the non-bonding orbital (or lone pair), the behavior of spin density is barely changing regardless whether the nuclei are allowed to move or not [128].

When nuclei are allowed to move, finally the charge transfer occurs. The ultrafast oscillatious stop due to decoherence caused by nuclear motion and the electron (hole) transfer from one site of the molecular system named donor to another site, an acceptor [129, 130, 131, 118]. Then the donor and acceptor of the molecule have positive and negative charge, which corresponds to the chemical reaction. The timescale of such process usually depends on the period of the involved nuclear vibration, thus occuring on nuclear timescale. Therefore, the pure electronically process CM can be regarded as an elementary step of charge transfer driven by nuclear motion. The detailed discussion can be found in Section III. 3.

The issue whether nuclear motion has an effect on the ultrafast transfer is a controversy for a long time and worth to be discussed. So, in general case both electronic and nuclear motion should be considered. In this work, we have taken the nuclear motion as a perturbation of the electronic system, regarding it as vibration bath. Therefore, relaxation and dephasing caused by nuclear motion are included as detailed in Sections II. 5, III. 6 and publication [**HW3**].

6 Spin Crossover

Another processes which has close relation to the topic of this work is SCO. It is a phenomenon occuring in some complexes consisting of TM ions and ligands with medium ligand field strength, involving the population transfer between a low-spin and a high-spin electronic states [132, 133, 134]. Thus, a spin-flip occurs. It can be triggered by external stimuli such as a variation of the temperature, pressure, and external magnetic field, and especially using light. It can lead to change of properties of material such as color, electrical resistance and magnetic moment. Optical stimulation is the most interesting way and has been studied in solutions [135] and in solids [136]. Several practical applications of such materials have

been suggested such as sensors, optical switches, displays, energy and information storage, energy transformation devices and nanophotonic devices. Besides, switchable liquid crystals and thin films of SCO materials have also been obtained [137, 138]. Devices based on spin-polarized currents could represent an advantageous extension of conventional electronics [139, 140], especially when talking about high-density magnetic data storage devices [138].

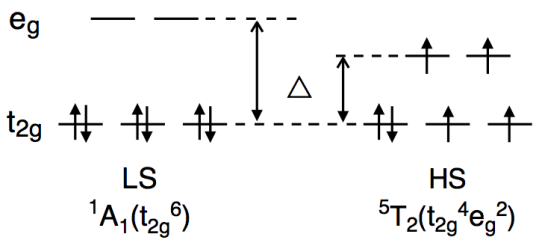

Figure I.3: The electron configuration for iron(II) in perfectly octahedral O_h coordination.

SCO phenomenon is commonly observed in the first-row TM complex with a d^4–d^7 electronic configuration in (near)octahedral ligand geometry. Those ions can exhibit different possible electron configurations. For instance, the d^6 electron configuration for Fe(II) is shown in Fig. I.3. This case is of particular interest for this work since Fe^{2+} ion has been selected as a test system [**HW1-3**]. Six electrons are in the five 3d shell orbitals which split into two groups belonging to t_{2g} and e_g irreducible representations. The former one is lower in energy than the latter due to smaller overlap with the ligands and thus experiencing less electron repulsion. They might be very close in energy, the value of the splitting is referred to as ligand-field splitting. It depends on several factors, including both the ligands and the metal ion, and the geometry of the complexes. Besides, whether the complex has a low-spin or high-spin electron configuration in the ground state is determined by the energy gap Δ and the spin-pairing energy. If Δ is greater than the spin-pairing energy of the complex, then the low-spin is more stable and the complex is less magnetic. Iron(II) and iron(III) polypyridine complexes in solution are popular SCO materials and have been widely investigated due to the partially filled 3d-shell of the iron atoms [82, 141, 132, 133, 142]. Moreover, this class of systems represents a prospective highly efficient light-harvesting and light-emitting materials for photovoltaics and photoelectronics, plays an important role in respiration, oxygen transport and photosynthesis and can be considered as a cheap and constituent for dye-sensitized

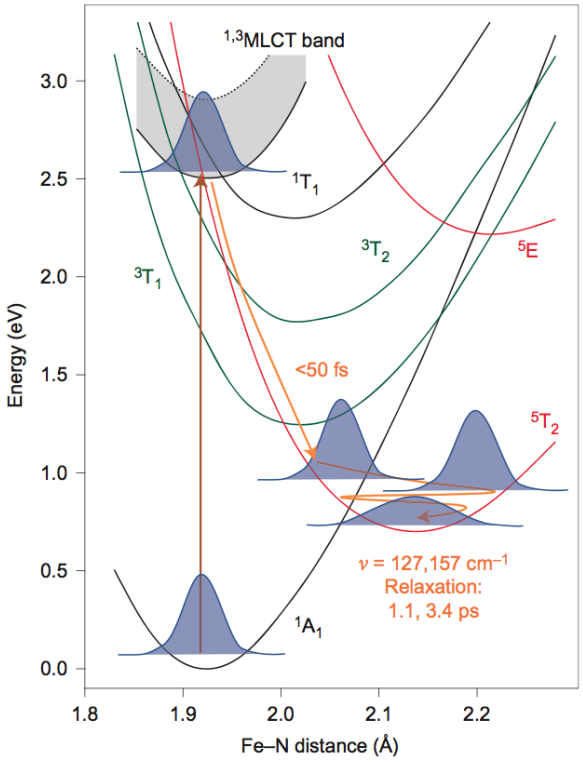

Figure I.4: Summary of the photoinduced SCO in $[Fe(bpy)_3]^{2+}$ occurring upon photoexcitation into the MLCT band [134]. Reprinted with permission from Springer Nature: G. Auböck, M. Chergui, Sub-50-fs photoinduced spin crossover in $[Fe(bpy)_3]^{2+}$, Nature Chemistry, 7, 629-633, (2015). Copyright 2015 Macmillan Publishers Limited. All rights reserved.

solar cells [143]. For these reasons, in our work, the prototypical Fe(II) complex $[Fe(H_2O)_6]^{2+}$was chosen to study the spin-flip and electron dynamics.

Spin crossover is a process driven by spin-orbit coupling. However, SOC between valence-excited states is very small. Upon valence excitation, an ultrafast SCO occurs when potential energy surfaces (PESs) of the excited states come close to each other. SCO takes place along the special configuration coordinate–a stretching mode which is corresponding to the elongation of the mental-ligand bonds [82, 83, 144, 145]. For example in Fig. I.4, the photo excited nuclear wave packet reaches and passes through the crossing region of the two nearly degenerate states with different multiplicity (^{1,3}MLCT and $^5T_{2g}$) within 50 fs. Then the molecule is cooled down within a few picoseconds. Therefore, SCO, although depending on the electronic SOC, is essentially a nuclear-driven process. Thus, the time scale is determined by the related vibrational periods.

For core-excitation when the related core-hole has non-zero angular momentum, the corresponding SOC increases dramatically, thus one could expect that an ultrafast purely electronically driven spin-flip process, which differs from the mechanism of the conventional SCO nuclear driven process, will occur. The relation between such a process and conventional SCO is similar to the relation between charge migration and charge transfer introduced in Section I. 5. The main focus of this work is put on spin-flip process; a detailed discussion can be found in Section III. 4.

To summarise, the bright attosecond pulses generated from HHG or XFELs provide a way to trigger and manipulate the ultrafast processes in time domain. These pulses can reach soft X-ray range and, thus, can be used to excite core electrons. It allows one to study complicated electron driven processes similar to CM and SCO initiated by X-ray light. In this work, simulations of such processes are considered in detail with special focus on spin-flip dynamics. The methodology and results are discussed in following Chapters.

Chapter II

Developed Theoretical Methodology

1 System-Bath Partitioning

In the following, a brief description of the theoretical method developed in this work is given. Since electron dynamics is mainly the focus of the present study, the Born-Oppenheimer approximation is used. Nuclei are fixed and the actual dynamics are studied at a single geometry of the molecule, namely, at the ground-state equilibrium position. With this we are assuming vertical excitation by the incoming light and also that the system is excited far from conical intersections. The timescale of such processes is in the range of only a few femtoseconds, which is much shorter than the periods of relevant metal-ligand vibrations. Hence, one can exclude nuclear dynamics under these circumstances. This situation is discussed in [**HW1**] and [**HW2**].

However, the environment (bath) may has an influence on the dynamics of the quantum system of interest: vibrations could still introduce decoherence and dephasing, as has been studied by Tremblay and Saalfrank et al. [4, 118, 146]. The details of this influence are strongly dependent on energy level structure of the system and the coupling between bath and system. In crudest approximation, nuclei are fixed, to go beyond we use perturbation theory in spirit of system-bath ansatz to account, at least approximately, for a possible influence of molecular vibrations and respective dephasing but also for loss channels such as Auger decay. The details are discussed in [**HW3**].

In the model used in this work, the total Hamiltonian is written as

$$\hat{H}(t) = \hat{H}_{\mathrm{S}}(t) + \hat{H}_{\mathrm{B}} + \hat{H}_{\mathrm{S-B}}\,. \tag{II.1}$$

It contains three parts: The first part, $\hat{H}_{\mathrm{S}}(t)$, describes the electronic degrees of freedom of the relevant system, whose dynamics is triggered by the X-ray light. The second part, $\hat{H}_{\mathrm{B}}$, is related to the degrees of freedom of the bath. The last part, $\hat{H}_{\mathrm{S-B}}$, describes the coupling between relevant system and bath. The dynamics of the relevant system according to its reduced density operator, $\hat{\rho}$, follows from the Quantum Master Equation [147, 4]

$$\frac{\partial}{\partial t}\hat{\rho} = -i[\hat{H}_{\mathrm{S}}(t), \hat{\rho}] + \mathcal{R}\hat{\rho} \; + \mathcal{A}\hat{\rho}\,. \tag{II.2}$$

Equation (II.2) assumes that the effect of the system-bath interaction can be treated in second order perturbation theory and invoking the Markov approximation. Here, $\mathcal{R}$ is the dissipation

superoperator, which accounts for phase and energy relaxation due to interaction with the vibrational bath and $\mathcal{A}$ accounts for the Auger decay. This equation was solved using the Runge-Kutta-Fehlberg integrator with adaptive step size.

2 Choice of the Basis

Within the density matrix-based time-dependent restricted active space configuration interaction (ρ-TD-RASCI) method, any convenient basis can be used depending on the process under study. At the lowest level is the configuration state function (CSF) basis, $\{\Phi_j^{(S,M_S)}\}$, with the total spin S and its projection M_S. Note that the relaxation of one-electron MOs is not taken into account and CSFs are constructed using a time-independent MO basis, optimized at the restricted active space self-consistent-field (RASSCF) level [148] prior to propagation. On this level, ρ-TD-RASCI method can describe electron correlation-driven processes analogous to CM in ionized species [**HW2**].

The system Hamiltonian in the CSF basis reads

$$\begin{aligned}\mathbf{H}_{\mathrm{S}}(t) &= \mathbf{H}_{\mathrm{CI}} + \mathbf{V}_{\mathrm{SOC}} + \mathbf{U}_{\mathrm{ext}}(t) \\ &= \begin{pmatrix} \mathbf{H}_h & 0 \\ 0 & \mathbf{H}_l \end{pmatrix} + \begin{pmatrix} \mathbf{V}_{hh} & \mathbf{V}_{hl} \\ \mathbf{V}_{lh} & \mathbf{V}_{ll} \end{pmatrix} + \begin{pmatrix} \mathbf{U}_h(t) & 0 \\ 0 & \mathbf{U}_l(t) \end{pmatrix},\end{aligned} \tag{II.3}$$

where blocks of low- (l) and high-spin (h) basis functions are seperated. In Eq. (II.3), $\mathbf{H}_{\mathrm{CI}}$ is the CI Hamiltonian matrix containing the effect of electron correlation. SOC is contained in $\mathbf{V}_{\mathrm{SOC}}$, whose matrix elements are calculated in the LS-coupling limit, making use of the atomic mean-field integral (AMFI) approximation [149], see Section II. 3. The interaction with the time-dependent electric field is

$$\mathbf{U}_{s=h,l}(t) = -\vec{\mathbf{d}}_{ss} \cdot \vec{E}(t), \tag{II.4}$$

which is taken in semiclassical dipole approximation with the transition dipole matrices $\vec{\mathbf{d}}_{hh}$ and $\vec{\mathbf{d}}_{ll}$ ($\vec{\mathbf{d}}_{hl} = \vec{\mathbf{d}}_{lh} = \vec{\mathbf{0}}$). $\vec{E}(t)$ is electric field of the incoming light pulse, see Section II. 4 for further details.

Besides, the other possibilities for the basis are spin free (SF) and spin-orbit coupling (SOC) states. Here, the eigenstates of $\mathbf{H}_{\mathrm{CI}}$ are called SF states, they are labeled by the set $\{\Psi_n^{\mathrm{SF},(S,M_S)}\}$, and can be expressed by linear combinations of CSFs, involving excitations from/to orbitals of interest:

$$|\Psi^{\mathrm{SF}}\rangle = C_0\,|\Psi_0\rangle + \underbrace{\sum_{ia} C_i^a\,|\Psi_i^a\rangle}_{\text{1h1p}} + \underbrace{\sum_{i<j,a<b} C_{ij}^{ab}\,|\Psi_{ij}^{ab}\rangle}_{\text{2h2p}} + \dots. \tag{II.5}$$

In this expression, $|\Psi_0\rangle$ represents the reference wave function of the ground electronic state and remaining terms are the single (1h1p), double (2h2p), etc excitations from the ground state configuration. Indices $i, j, \dots$ denote occupied MOs from which electron is excited to unoccupied $a, b, \dots$ ones.

The SOC states are defined as the eigenstates of $\mathbf{H}_{\mathrm{CI}} + \mathbf{V}_{\mathrm{SOC}}$ and consequently are linear combinations of spin frees (SFs):

$$|\Psi_a^{\mathrm{SOC}}\rangle = \sum_n C_{an}^{(S,M_S)} |\Psi_n^{\mathrm{SF},(S,M_S)}\rangle \ . \tag{II.6}$$

Matrices $\boldsymbol{\rho}$ and $\mathbf{H}$ can be easily converted between these bases, but propagation in either of them has its advantages. SF basis is convenient to be used in the study of spin dynamics which is detailed in the Sections III. 4 and III. 5. SOC states are convenient to be used in the spin dynamics accounting for the dissipative part which is discussed in Sections II. 5 and III. 6. As already mentioned CSF basis is convenient to study electron correlation-driven processes.

3 Electronic Structure Method

Two electronic structure methods are essential for this work: RASSCF and AMFI. The CSFs are constructed within a RASSCF scheme [150, 151, 152] which is a general approach to describe the electronic structure of a system using the active space strategy. RASSCF employs, e.g., CSF-based algorithms to solve the configuration interaction problem. It can be regarded as the combination of the Hartree-Fock (HF) and full CI method which uses a linear combination of CSF to approximate the exact electronic wavefunction of an atom or a molecule. In this method, the wavefunction has high flexibility: since both the electron correlation and the orbital relaxation are taken into account. Since the number of CSFs quickly increases with the number of active orbitals, the computational cost increases accordingly. We restrict the number of electrons and the relevant orbitals in certain subspaces (RAS1-RAS3) to construct the electronic configurations, as shown in Fig. II.1. The orbitals were optimised in the state-averaged way to ensure the convergence.

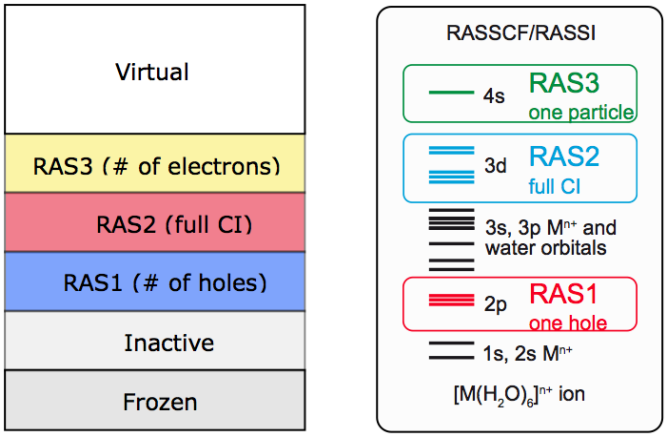

Figure II.1: A scheme of RASSCF active space for $[\mathrm{M(H_2O)_6}]^{n+}$.

SOC between the different electronic states can be calculated using the state-averaged multi-configurational self-consistent-field method (MCSCF) [153] and the multi-reference configuration interaction method [154, 155] as well as MCSCF response theory method. In general, an effective mean-field spin-orbit Hamiltonian was used. It is based on atomic mean-field integral (AMFI) [149], which avoids the calculation of multi-centre one- and two-electron spin-orbit integrals and thus can take advantage of the full spherical symmetry. Thus, it drastically reduces the computational effort with negligible loss of accuracy. The spin-orbit coupling Hamiltonian can be expressed in the Breit-Pauli form in atomic units [156]:

$$\hat{H}_{\mathrm{SO}} = \frac{1}{2c^2}[\sum_{i\alpha} Z_\alpha \hat{\vec{s}}_i(\frac{\hat{\vec{r}}_{i\alpha}}{r^3_{i\alpha}} \times \hat{\vec{p}}_i) - \sum_{i\neq j}(\frac{\hat{\vec{r}}_{ij}}{r^3_{ij}} \times \hat{\vec{p}}_i) \cdot (\hat{\vec{s}}_i + 2\hat{\vec{s}}_j)] \,. \tag{II.7}$$

The first part is the one-electron term, where the electron is moving in the field of the nuclei with charge Z_α. In Eq. II.7, $\hat{\vec{s}}$ is spin and $\hat{\vec{p}}$ is the orbit momentum operator for ith electron. $\hat{\vec{r}}_{i\alpha}$ is the distance between the ath nucleus and the ith electron and c is the light speed. The second part is the two-electron term which describes the coupling of orbital momentum of ith electron with the spin of jth electron. Within the AMFI approximation, the SOC Hamiltonian in MO basis ($|i\rangle$, $|j\rangle$, $|k\rangle$) reads as follows [149],

$$V_{ij} = \langle i|\hat{h}|j\rangle + \frac{1}{2}\sum_k n_k\{\langle ik|\hat{g}|jk\rangle - \langle ik|\hat{g}|kj\rangle - \langle ki|\hat{g}|jk\rangle\} \,, \tag{II.8}$$

where $\hat{h}$, $\hat{g}$ are the one- and two-electron operators, and n_k denotes the occupancy of the orbitals. n_k are set to be occupation number of the isolated neutral atoms. Thus, only SOC within the atoms of a molecule is taken into account. Further, only the direct SOC is considered in this work, that is why the coupling between the states should fulfil the selection rule $\Delta S = 0, \pm 1$.

4 Light-Matter Interaction

Two types of light pulse have been considered in this work. Isolated pulses modelling XFEL output, were discussed in [**HW1**]. They can be expressed as $\vec{E}(t) = \vec{e}E_0 \exp(-t^2/(2\sigma^2))\cos(\Omega t)$. Pulse trains, modelling HHG output and discussed in [**HW3**], read as $\vec{E}(t) = \vec{e}E_0 \sum_i \exp(-(t-t_i)^2/(2\sigma^2))\cos(\Omega t)$. The electric field $\vec{E}(t)$ entering the Eq. II.4 is determined by polarization $\vec{e}$, amplitude E_0, carrier frequency Ω and Gaussian envelope with width σ. The parameter t_i corresponds to the center of peak of ith subpulse in a train. The influence of carrier-envelope phase can be neglected for the carrier frequency in X-ray range, because of the multiple oscillations occur within a single pulse. The envelope of the pulse train $\tilde{E}(t) = E_0 \sum_i \exp(-(t-t_i)^2/(2\sigma^2)$ is depicted in Fig. II.2, showing also the parameters E_0, t_i and σ. T is the period of the optical cycle of the driving laser in HHG setup. The shape of the time-dependent external electric field has been chosen to roughly resemble the regimes of XFELs and of the commonly used driving laser systems for the HHG, see also discussion in Sections I. 3 and I. 2. However, some assumptions on the form of the electric field have been done allowing to simplify the computational protocol for HHG. We have chosen 400, 800, 1400 and 2000 nm as the wavelength of the driving laser. Here, 800 nm corresponds to the Ti:Sapphire laser. Other cases (400, 1400, and 2000 nm) can be obtained by frequency doubling and parametric amplifiers of Ti:Sapphire laser. The value of $t_i - t_{i-1}$ corresponds to the time distances between consecutive subpulses which is in the range from about 1 to 7 fs. The wavelength λ of the driving pulse

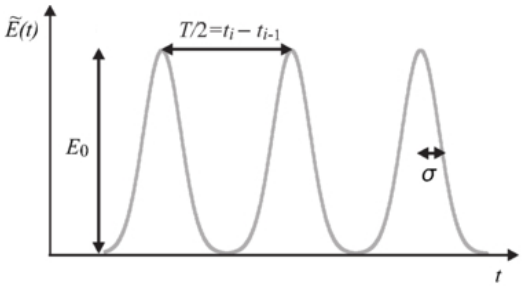

Figure II.2: Scheme explaining the parameters of the light pulse train envelope.

is the most important parameter because it fixes $t_i - t_{i-1}$ and σ. Moreover, we assume that σ can be controlled filtering out the low-energy harmonics of the HHG output. Otherwise, it would be bound to the inverse of the cutoff energy. In our model, the duration of subpulses has been chosen to depend on the period ($\sigma = T/14$ and $T/28$), for more details see discussion in [**HW3**]. We have performed systematic screening of the parameters in [**HW2**] and [**HW3**]. For simplicity, the simulation employs ten pulses in each series and assumes equal envelopes of the subpulses.

It should be noticed that despite the large values of E_0 (corresponding intensities of 0.25 – 2.5 a.u. or $8.8{\times}10^{15}\,\mathrm{W/cm^{-2}}$ – $8.8{\times}10^{16}\,\mathrm{W/cm^{-2}}$) used in this work, at soft X-ray wavelength this corresponds to the weak field regime, see [**HW1**] and [**HW2**]. In most cases listed in the thesis, the polarization vector $\vec{e}$ has been chosen to be parallel to the shortest Fe–O bond of the employed model, i.e. the $[Fe(H_2O)_6]^{2+}$complex, see also Section III. 5.1.

One should keep in mind that both the single pulse and the trains of ultrashort pulses in our theoretical study have been designed solely for illustration purposes and correspond to realistic experimental setups only approximately. However to the best of our knowledge, such a setup is not yet available. The duration of the X-ray pulse generated from XFELs ranges from a few to about 100 fs [40]. Although the time-duration is reachable by HHG, the intensity of the output from HHG is of the order of $10^{12}\,\mathrm{W/cm^{-2}}$. When isolated pulses are generated by HHG, they are of even lower intensity.

5 Dissipative Dynamics

Dissipative dynamics, has been considered only in [**HW3**], whereas [**HW1,2**] describe closed system quantum dynamics. Two processes are considered, i.e. electron-vibrational coupling and Auger decay. First, let us focus on the superoperator $\mathcal{R}$ which describes the effect of electron-vibrational coupling. The vibrational bath is assumed to be a collection of harmonic oscillators in thermal equilibrium coupled to the electronic transitions in a Huang-Rhys like fashion [147]. This constitutes the primary vibrational bath with the interaction operator

$$\hat{H}_{\mathrm{el-vib}} = \sum_{ab} \sum_{\xi} g_{ab,\xi} \omega_\xi Q_\xi \left|\Psi_a^{\mathrm{SOC}}\right\rangle \left\langle\Psi_b^{\mathrm{SOC}}\right| , \tag{II.9}$$

where a and b label the coupled electronic SOC states and Q_ξ is the coordinate of the normal mode ξ having frequency ω_ξ. Here, $g_{ab,\xi}$ is the dimensionless shift of the a's state harmonic potential energy surface with respect to the potential of state b, which can be expressed by the Huang-Rhys factor $S_{ab,\xi} = g_{ab,\xi}^2/2$.

This primary bath describing the system is coupled to a secondary one (further solvation shells) leading to a multi-mode Brownian oscillator model [157]. In total, the effect of primary and secondary bath can be described by the following spectral density

$$J_{ab}(\omega) = \sum_{\xi} \omega_\xi^2 g_{ab,\xi}^2 \frac{\omega\omega_\xi\gamma}{(\omega^2 - \omega_\xi^2)^2 + \omega^2\gamma^2} , \tag{II.10}$$

where the parameter γ accounts for the influence of the secondary bath.

For simplicity, we have restricted ourselves to the Bloch model which decouples population

relaxation and coherence dephasing. In this case, the only non-zero elements of the relaxation matrix (Redfield tensor) $\mathcal{R}_{ab,cd}$ are given by

$$\mathcal{R}_{aa,cc} = -\delta_{ac} \sum_e k_{a\to e} + k_{c\to a} \tag{II.11}$$

for population relaxation and

$$\mathcal{R}_{ab,ab} = -\frac{1}{2}(\sum_e k_{a\to e} + \sum_e k_{b\to e}) \tag{II.12}$$

for coherence dephasing.

The relaxation rates $k_{a\to b}$ for the transition from a state $|\Psi_a^{\mathrm{SOC}}\rangle$ to a state $|\Psi_b^{\mathrm{SOC}}\rangle$, can be expressed as

$$k_{a\to b} = 2[1 + n(\omega)][J_{ab}(\omega) - J_{ab}(-\omega)]\,, \tag{II.13}$$

where $n(\omega) = (\exp(\omega/k_{\mathrm{B}}T) - 1)^{-1}$ is Bose-Einstein distribution function.

Auger autoionization, is known to dominate the population decay for L-edge states of early transition metals. That is why radiative spontaneous emission has not been included as it has less than 1% contribution [158]. Auger decay is incorporated phenomenologically by the decay rate Γ_a yielding the simple Auger decay matrix

$$\mathcal{A}_{ab,cd} = -\delta_{ab}\delta_{cd}\delta_{ac}\Gamma_a\,. \tag{II.14}$$

Notice that this term is not norm-conserving. The rates Γ_a, were set to 0.4 and 1.04 eV for the L_3 and L_2 edges, respectively [159]. These values correspond to lifetimes of the core hole of 10.3 and 3.98 fs.

Chapter III

Results and Discussion

1 Model System

In my work, the approach described in the previous Chapter is applied to $[Fe(H_2O)]^{2+}$ complex for several reasons. Firstly, it is a typical TM complex, representing a Fe^{2+} ion containing salt in water solution with its first solvation shell. Next, the X-ray absorption L-edge of the Fe^{2+} is in soft X-ray range, so HHG light sources can be used for excitation. Further, its half-filled $3d$ shell has both strong electron correlation and features high/low spin states. Besides, the SOC of the created $2p$ core-hole is strong leading to prominent spin dynamics. These dynamics is essentially the main focus of my work. Last but not least, according to our experience with other TMs compounds [160, 161, 162], the spin-flip phenomenon should be relevant for all systems with core-holes with nonzero angular momentum. That is why the phenomena discussed here for $[Fe(H_2O)_6]^{2+}$have a broader scope.

The ground electronic state of $[Fe(H_2O)_6]^{2+}$has a quintet ($S = 2$) high spin d^6 electronic configuration leading to triple degeneracy if octahedral symmetry is assumed. This degeneracy is lifted due to the weak Jahn-Teller effect, resulting in the three close-lying electronic states. Due to zero-field SOC splittings these three quintet states are slightly split giving rise to 15 micro-states which can be thermally populated at ambient temperature, see Section III. 2. As shown in panel b) of Fig. III.1, an active space containing 12 electrons distributed over the three $2p$ (1 hole is allowed) and five $3d$ (full CI) orbitals has been used, to describe the core excited electronic states corresponding to the dipole allowed $2p \rightarrow 3d$ transitions [160, 163, 162]. This active space included up to 4h4p configurations, and in total, resulted in 35 quintet ($S = 2$) and 195 triplet ($S = 1$) electronic states, directly interacting via SOC according to the $\Delta S = 0, \pm 1$ selection rule. Accounting for the different M_S components, the total amount of the SF and SOC states was 760, where 160 are valence and 600 core ones. The second-order Douglas-Kroll-Hess transformation was used to account for scalar relativistic effects [164]. This setup was employed in all three publications [**HW1-3**]. However, in [**HW2**] we also studied the influence of inclusion of singlet states which corresponds to a second-order SOC effect.

The L-edge X-ray absorption spectrum is shown in panel a) of Fig. III.1. The accuracy of the electronic structure method can be judged by comparison of calculation (red) with experiment (blue). As can be seen from Fig. III.1 a), the agreement is very good given the fact that line broadenings have not been explicitly fitted to experiment. The spectrum has

a shape characteristic for transition metals, featuring the L_3 (J = 3/2) and L_2 (J = 1/2) bands split due to the SOC. This splitting is 12.7 eV what corresponds to a timescale of about 0.33 fs. The arrows labeled 1, 2, 3 denote the carrier frequencies $\hbar\Omega$ of the laser fields used for excitation, see Section II. 4. These labels 1, 2, 3 are consistent with the labels used in the panel a) of Fig. III.2 for state ranges. These ranges demonstrate the scope of the electronic states lying within the FWHM bandwidth of the excitation pulses discussed below. Thus, one can assume that these states are notably excited by the incoming light pulses. More detailed discussion is given in following Sections III. 4 and III. 5. The frequency combs corresponding to HHG with the respective wavelengths of the driving laser, are also shown and are considered in Section III. 5.

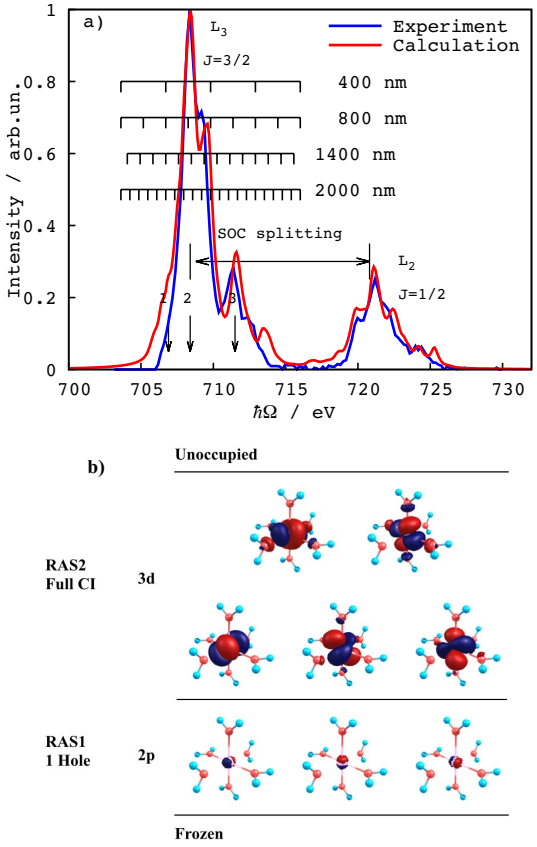

Figure III.1: a) Calculated X-ray absorption spectrum of $[Fe(H_2O)_6]^{2+}$(red line), as compared to experiment (blue line) (partial electron yield from 2p3d3d channel [162]). Arrows mark the energies corresponding to carrier frequencies $\hbar\Omega$ =706.9, 708.4 and 711.5 eV. The frequency combs corresponding to HHG with the respective wavelengths of the driving laser are also shown. b) MO active space for the ρ-TD-RASCI calculation.

2 Considered Dynamic Regimes

In the following, we will discuss five different excitation regimes, illustrating the dynamics of ultrafast spin-crossover. In *regime I* [**HW2**], we consider the effect of electron correlation which is quite substantial for core-excited states. Thus, we consider the case where $\mathbf{H}_{\mathrm{CI}} \neq 0$, $\mathbf{V}_{\mathrm{SOC}} = 0$ and $\vec{E}(t) = \vec{0}$, see Eq. II.3. In this case, an instantaneous population of a particular CSF is addressed, being a superposition of SF eigenstates. In principle, it resembles the CM studies [80, 102, 100, 103, 104, 105, 106, 107, 108] with the difference, that dynamics occur after electron excitation but not ionization.

In *regime II* [**HW1,2**], we study the ultrafast spin-flip dynamics driven solely by SOC, here only $\vec{E}(t) = \vec{0}$ in Eq. II.3. Hence, a particular SF state, which is a superposition of strongly spin-mixed $2p$ core-hole states, is initially prepared. Such situation is of a purely theoretical interest, since it can hardly (if at all) be realised in experiments.

In *regimes III* and *IV*, we design a possible experimental setup to study such ultrafast electronically driven SCO, considering a situation of excitation by an explicit field. The system is initially in an incoherent mixed state. The 15 M_S microstates of the lowest closely lying electronic states are populated according to the Boltzmann distribution at 300 K. The initial density matrix reads

$$\boldsymbol{\rho}_0 = \mathrm{diag}\{Z^{-1}\exp(E_i/kT)\}, \tag{III.1}$$

where $Z = \sum_i \exp(E_i/kT)$ is the partition function. The core-hole is created, and the spin dynamics are driven by a single ultrashort X-ray pulse (*regime III*) [**HW1,2**] and pulse trains (*regime IV*) [**HW3**]. These regimes correspond to a possible experimental realization using XFELs or HHG radiation, respectively.

In *regime V* [**HW3**], we account for the influence of the dissipation. Here, we focus on the electron-vibrational coupling, treated at the level of system-bath partitioning, see Section II. 5.

3 Electron Correlation-driven Dynamics

In *regime I*, the electron correlation-driven dynamics, analogous to CM discussed in Section I 5, is considered. The detailed description of this regime is published in [**HW2**]. In order to study the effect of the electron correlation separate from the SOC, an instantaneous preparation of a particular CSF belonging to the quintet manifold is assumed. Here, the chosen excited electronic configuration, CSF 9, corresponds to the largest contribution to the SF_{core} state considered in Section III. 4. As illustrated in panel a) of the Fig. III.3, the propagation of the impulsively excited CSF 9 leads to fast redistribution of CSF populations within 15 fs. The ultrafast decay of the initial CSF 9 population has multiple revivals within this time period. These dynamics indicate the strong electron correlation in the core-excited states. In general, the timescale of such dynamics is faster than that of the core-hole migration phenomena observed for ionized systems [106]. That can be explained by the fact that for $2p$ hole together with the half-filled $3d$ shell, the electron correlation is stronger than for $1s$ or $2p$ hole-state of the second period elements. For the valence excited states as shown in the Fig. 5 b) of [**HW2**], the dynamics is slightly modulated by the coherences with other electronic configurations within the first 15 fs and the oscillation period is much longer than for the core-excited states. Such behavior results from the weaker electron correlation in the valence-excited states.

In conclusion, electron correlation is important for the electron dynamics in the core-excited states of TM complexes. The developed method can be used in this regime to simulate the CM processes and study the dynamics solely driven by electron correlation. In cases when valence electronic states are involved, such applications might be relevant to studies of the TM-based molecular electronic devices [165]. However, the main focus in this work is put into spin dynamics as discussed in following section. We will thus not return to the discussion of electron correlation.

4 Spin-Orbit Coupling-driven Dynamics

The *regime II*, featuring the ultrafast spin-flip dynamics driven solely by SOC has been discussed in [**HW1**] and [**HW2**]. For valence excited states, the SOC is weak. Thus, the SCO is essentially driven by nuclear motion since it requires the nuclear wavepacket to pass through a region of near-degeneracy of two states of different multiplicity [166], see Fig. I.4 in Chapter I. Usually the timescale of such ultrafast SCO is determined by the related vibrational periods which are around 100 fs [133, 134, 167]. However, for core-excited electron levels, the corresponding magnitude of SOC increases dramatically and is strong enough to drive the spin-flips, even before nuclear motion sets in. Instead, the spin dynamics is expected to be an electronically driven process.

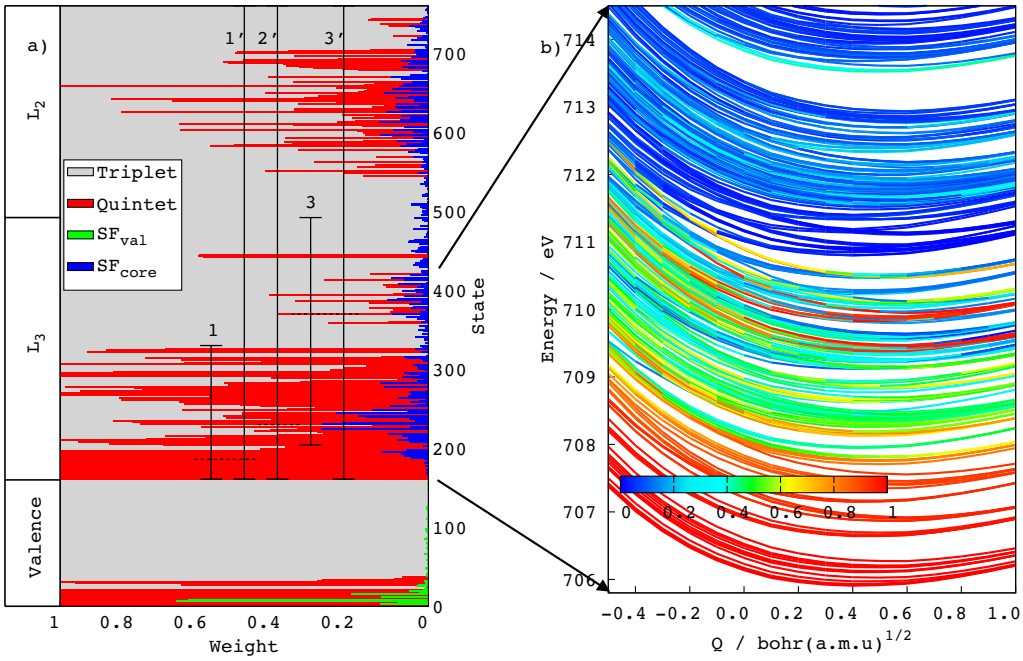

Figure III.2: a) Collective contributions of the quintet (red bars) SF states to the stationary SOC eigenstates; the grey areas correspond to the triplet SF states counterpart. The total contributions of these two parts sum up to unity. The particular contributions of valence SF (SF_{val}, green bars) and core SF (SF_{core}, blue bars) states used in regime II to the different SOC states are also shown. Numbered ranges reflect the bandwidths of 31.4 eV (1,3) and 3.1 eV (1'–3') pulses with carrier frequencies denoted in panel (a) of Figure III.1 in terms of the involved SOC states. b) The core potential energy surface (PES) in SOC basis along the most active tuning vibrational mode (ground state frequency 417 cm^{-1}). The color indicates the change of the multiplicity of the states from quintet (red) to triplet (blue).

It is demonstrated for the first time in [**HW1**] that electronically driven SCO after core-hole excitation in TMs indeed takes place on a few femtoseconds time scale, as shown in the panel b) of Fig. III.3. The idea of this case is to prepare a superposition of the $2p$ core-hole excited SOC states, such that it represents a pure SF state SF_{core}. Such superposition is non-stationary under action of $\mathbf{H} = \mathbf{H}_{CI} + \mathbf{V}_{SOC}$ and undergoes ultrafast dynamics.

Here, the peculiarities of spin-mixing with our LS-coupling scheme are essential. Fig. III.2 a) shows the weights of the quintet (red) and triplet (grey) states for each SOC state. The valence-excited SOC states which are lying at lower energies are mostly pure quintets or triplets. In contrast, the core-excited SOC states are dominantly spin mixtures, with the degree of spin-mixing varying with state energy. This fact further demonstrates that the SOC strength for core-excited states is larger than for the valence-excited ones. The contributions of SOC states to the selected representative initial states F_{core} are also labeled with blue bars In Fig. III.2 a). It shows that SF_{core} is essentially a superposition of all 600 SOC core states considered here.

In the panel b) of Fig. III.3, the total populations of all quintet and triplet SF states with (blue and red solid lines) and without (brown and green solid lines) Auger decay are shown within 15 fs for a representative quintet SF core state. It can be seen in Fig. III.3 b), for the case without Auger decay, that the total population of the quintet states drops while the one for triplets is increasing within first few femtoseconds. After around 1 fs, the total triplet population

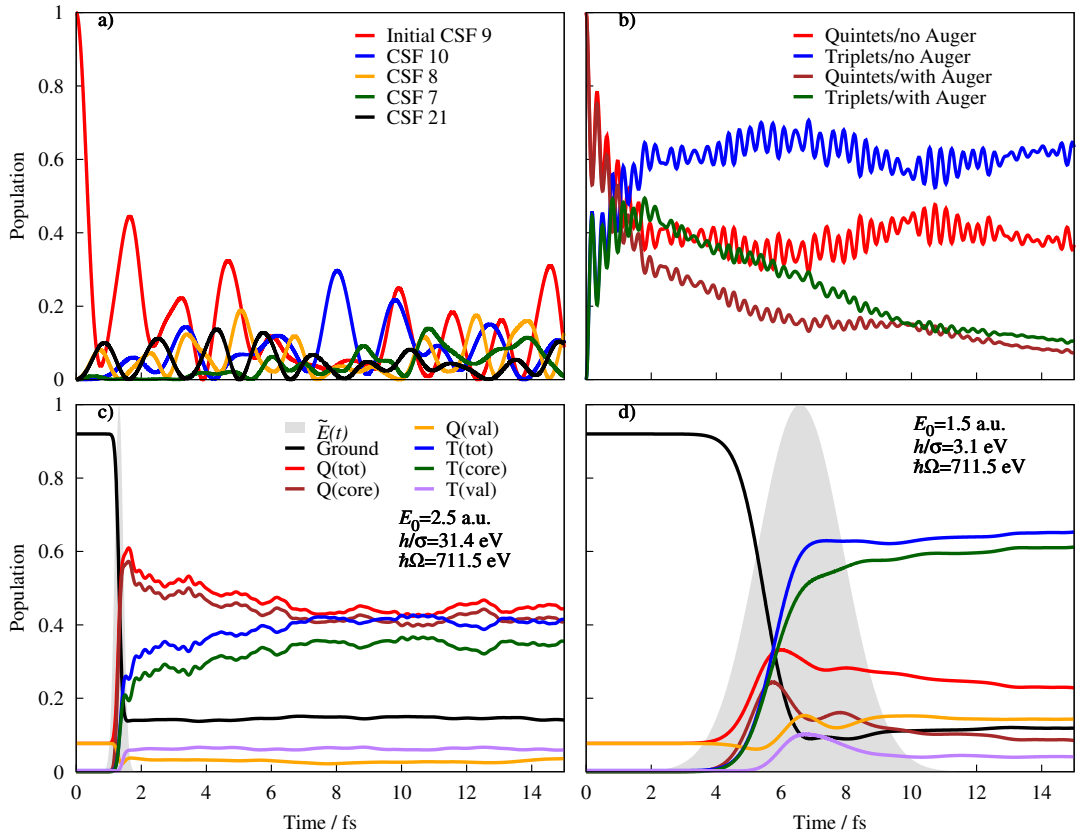

Figure III.3: a) *Regime I*, the population dynamics initiated by the instantaneous preparation of CSF 9. b) *Regime II*, evolution of the total population of the quintet ($S = 2$) and triplet ($S = 1$) electronic states after instantaneous excitation to a SF_{core} state with and without Auger decay. The decomposition of this SF_{core} state into SOC states is shown in Fig. III.2 a) (blue bars). c) and d) *Regime III*, spin dynamics initiated by explicit field excitation with carrier frequency 711.5 eV and with different field amplitudes and bandwidths corresponding to: c) E_0 =2.5 a.u. and 31.4 eV, d) E_0 = 1.5 a.u. and 3.1 eV.

becomes larger than the quintet one, thus spin-flip has occured.

The main contribution to such fast drop of the population of the total quintets is due to the $(S = 2, M_S = +2) \rightarrow (S = 1, M_S = +1)$ transitions. After about 1 fs, quintets with $M_S = -1$ and -2 start to be populated. Then about 4 fs later, the system reaches almost a stationary situation and the populations of M_S components oscillate around their mean value. The fast modulations with a period of 0.32 fs as shown in panel b) can be assigned to the SOC splitting between the L_2 and L_3 bands. This is an intrinsic property of the $2p$ core-hole. If one compares first few femtosecond dynamics to the case with Auger decay, the total population of quintets drops and the triplet one increases, similar to the case without Auger decay. After spin-flip occurs, a biexponential decay of the populations takes place, which depends on the choice of the two decay parameters, Γ_a, in Eq. II.14 common for all L_2 and L_3 states.

For the initially prepared valence-excited SF states, the corresponding spin dynamics has also been studied in [**HW2**]. Because of the rather weak SOC, almost no spin dynamics happens within the first 15 fs. Therefore, the initial condition where valence-excited states are instantaneously prepared will not be discussed further.

To sum up, one can conclude that the spin-flip occurs faster than the Auger decay with

a time constant of 4 fs. The core-excited states demonstrate intricate fast purely electronic spin-flip dynamics which is solely driven by strong SOC. The timescales for such processes is two orders of magnitude faster than that driven by nuclear motion in conventional SCO [134]. However, the initial conditions used so far are quite artificial and would require complex-shaped elliptically polarized pulses with sub-200 as duration. In this work, this regime will serve as a reference to highlight the spin dynamics solely driven by SOC, more realistic situations are considered below.

5 Explicit Field Excitation

5.1 Single Pulse

Regime III, is designed to approximately resemble a possible experiment to study such ultrafast electronically driven SCO [**HW1,2**]. Here, we considered a situation of excitation by a single X-ray ultrashort pulse with Gaussian envelope, and linear polarization. Such regime is modelling XFEL excitation. In this regime, we have chosen carrier frequencies $\hbar\Omega = 706.9, 708.4, 711.5\,\text{eV}$ which are labeled (1-3) in the panel a) of Fig. III.1 with arrows. They correspond to the peaks in the X-ray absorption spectrum. The corresponding pulse bandwidth $h/\sigma = 31.4\,\text{eV}$ is reflected by numbered ranges 1-3 and 3.1 eV with 1'-3' shown in panel a) of Fig. III.2. This numbered intervals mark the range of the core-excited SOC states covered by the corresponding X-ray pulse. These chosen frequencies correspond to spectral regions with different quintet-triplet spin mixing (panel a) of Fig. III.2). The amplitudes for different excitation pulses have been chosen to give a similar depletion of the ground states of about 80%. In Fig. III.3, the results for only two excitation conditions are shown: the pulse with carrier frequency $\hbar\Omega = 711.5\,\text{eV}$ for both cases, bandwidth $h/\sigma = 31.4\,\text{eV}$ and amplitude $E_0 = 2.5\,\text{a.u.}$ for panel c) and $h/\sigma = 3.1\,\text{eV}$ and $E_0 = 1.5\,\text{a.u.}$ for panel d). The pulse envelopes are depicted with grey filled curves. The populations of the SF states for total-, valence- and core-states for quintet multiplicity, Q(tot), Q(val) and Q(core), as well as for triplet, T(tot), T(val) and T(core), are presented in the panel c) as depicted with different color curves. The black curve corresponds to the population of ground states, the initial population of 0.92 results from the Boltzmann distribution at the finite temperature of 300 K. For panel c) when the pulse comes in, the ground state depletion results in a fast increase of population of quintet states. After a short delay triplets are also populated. The quintet population drops down and at the same time the triplet one increases. After about 7 fs the total quintet and triplet populations oscillate near some equilibrium values. For different excitation condition, the oscillatory behavior of populations is still similar but actually has different period of modulation. If compared to the *regime II*, similar spin dynamics happens, however, the notable difference is the absence of rapid oscillations. It is due to the effect of the pulse with temporal width larger than the modulations with the oscillation period of about 0.3 fs. For panel d), as the bandwidth of the pulses further decreases, the oscillations are gradually eliminated and the triplet population increases quickly and even becomes larger than the quintet one. The quintet/triplet ratio at 15 fs is sensitive to the carrier frequency and width of the pulse, and it changes from 0.4 to 11.3 depending on pulse parameters as discussed in [**HW1**]. This selectivity can be used to control the spin mixing.

From this study, it is concluded that soft X-ray pulses can be used to trigger and control the ultrafast spin dynamics, which is faster than the 2p core-hole lifetimes. However, the field intensity used in this regime with the magnitude of about $10^{17}\,\mathrm{W/cm^{-2}}$ is barely accessible in synchrotron X-ray setups [168]. Further, due to the fact that the pulse duration from the XFELs is larger than 20 fs, they currently can not initiate and follow the ultrafast spin dynamics in this regime. We believe that further developments will enable the observation of this effect in nearest future.

5.2 Pulse Trains

In *regime IV*, we consider using pulse trains which contain ten identical subpulses with the polarization along the shortest Fe–O bond. This regime is modelling the HHG pulse trains which are easier to generate than the isolated pulses, see Section II. 4. Such regime is discussed in [**HW3**]. The corresponding spin dynamics triggered by the soft X-ray pulse trains are depicted in Fig.III.4. Here we have chosen four wavelengths of pump laser: 400, 800, 1400, and 2000 nm. 800 nm correspond to the wavelength of Ti:Sapphire, and 400, 1400, and 2000 nm can be obtained by frequency doubling and parametric amplification of the Ti:Sapphire 800 nm laser. The intervals between subpulses and the width of subpulse are determined by these choices. The pulse parameters of the HHG frequency combs generated with different driving lasers overlaid with the spectrum are shown in panel a) of Fig. III.1. In this Figure, it can be seen that the carrier frequencies $\hbar\Omega$ have been chosen not to fit to harmonics of the driving laser exactly, but rather correspond to resonances for convenience. However, there is only slight difference between the chosen "resonant" carrier frequencies and the exact positions of the harmonics for the cases of 800, 1400, 2000 nm. But for 400 nm there is a notable deviation between them.

Comparing the dynamics triggered by isolated pulse (solid lines in panel III.4 a)) during the first pulse in a sequence in panel c) the behavior is almost identical. At later times the population curves are naturally different. For single pulse it corresponds to the coherent electronic wave packet evolving in time according to the field-free Hamiltonian. In contrast, pulse trains constantly prepare new coherent superpositions and smear the populations of valence- and core-excited states in the process of absorption and stimulated emission. In general, it can be stated that the characteristics of the single pulse in the train have less influence on the dynamics than for the isolated pulse.

From the panels b)-d) in Fig. III.4, the spin dynamics triggered by pulse trains with different parameters are presented, using the same colors to label the corresponding populations as in the *regime III* (Fig. III.3). One can see similar effects on the spin dynamics driven by the pulse trains as has been demonstrated for the regime of isolated pulse. Note that between each subpulse ultrafast dynamics occurs, especially core states of both triplet and quintet multiplicity have a obviously stepwise rise and decrease behavior with every incoming pulse. The height of each step is gradually decreased, and after about five or six pulses reaches saturation. For the strong pulse, the valence excited states could gain a substantial population reaching up to the 35% of the total population, which may be attributed to stimulated emission. For weak pulses, the population of the valence states is almost constant and is less than 10%, and the stimulated emission effect almost disappears.

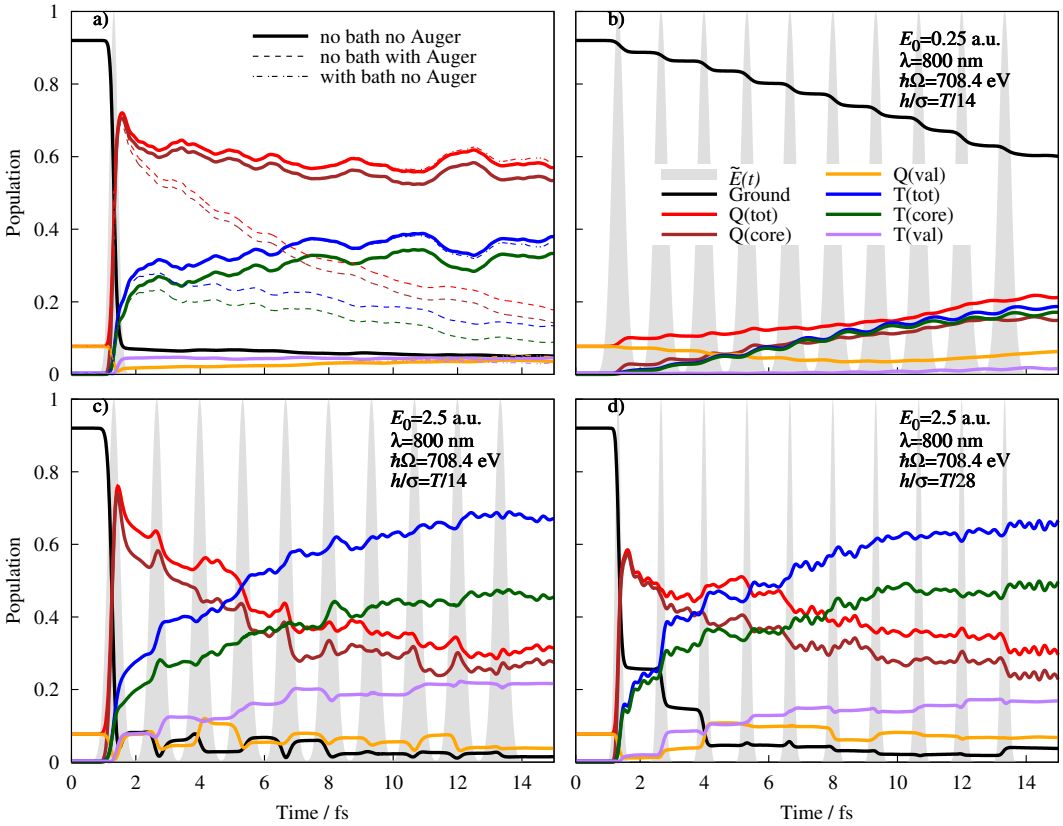

Figure III.4: *Regime IV*, the total populations of quintet, Q(tot), and triplet, T(tot), as well as of the respective valence, Q(val) and T(val), and core, Q(core) and T(core), electronic SF states simulated in different regimes. The shape of the normalized pulse envelope is depicted with grey filled curves. Black curve corresponds to the population of the lowest quintet (ground) state. (a) Spin dynamics initiated by single pulse with amplitude E_0 =2.5 a.u., carrier frequency $\hbar\Omega$ = 708.4 eV, bandwidth h/σ =31.4 eV, no bath, with (dash lines) and without (solid lines) Auger decay. The case with bath, no Auger decay is depicted by the dash-dotted linespanels (b-d) Spin dynamics initiated by pulse trains with different characteristics. The amplitude for b) is 0.25 a.u. while for c) and d) are 2.5 a.u., for all this three panels the carrier frequency are 708.4 eV and wavelength of the driving laser λ =800 nm, the subpulse duration for b) and c) are $\sigma = T/14$, for d) are $\sigma = T/28$, where T is a period of the driving pulse optical cycle.

The essential spin dynamics does not crucially depend on the pulse strength. That statement can be illustrated by analysis of the obtained T/Q ratio in terms of the applied pulse intensity. In Fig. III.5, the triplet/quintet ratio T(tot)/Q(tot) versus the integrated intensity with respect to the envelope $I_i = \int_{-\infty}^{(t_{i+1}-t_i)/2} |\tilde{E}(t)|^2 dt$ is depicted. Panels a) and b) illustrate cases for $\lambda = 800$ and 2000 nm, respectively. In order to increase the overlap along x-axis between $E_0 = 0.25$ and 2.5 a.u. branches, we subdivided the first pulse in a sequence for $E_0 = 2.5$ a.u., and applied longer pulse sequences for $E_0 = 0.25$ a.u. without Auger decay. The respective data points are depicted by the filled circles only for $E_0 = 2.5$ a.u.. The data with and without Auger decay were plotted with dashed and solid lines. Panel c) shows the results for $\sigma = T/14$, with different λ and $\hbar\Omega$. Analysing the results, the dependencies can be divided into four mostly linear regions: i) rise, mainly seen during the first pulse for $E_0 = 2.5$ a.u.; ii) rise with high steepness most apparent for $E_0 = 0.25$ a.u.; iii) rise with lower steepness; iv) saturation region which can be followed by decrease or oscillatory behavior of the T/Q ratio. The region iii) with lower steepness begins

when the triplet population starts to dominate over the quintet one. That is why it can be attributed to the interplay of the absorption/emission and Q→T/T→Q forward and backward

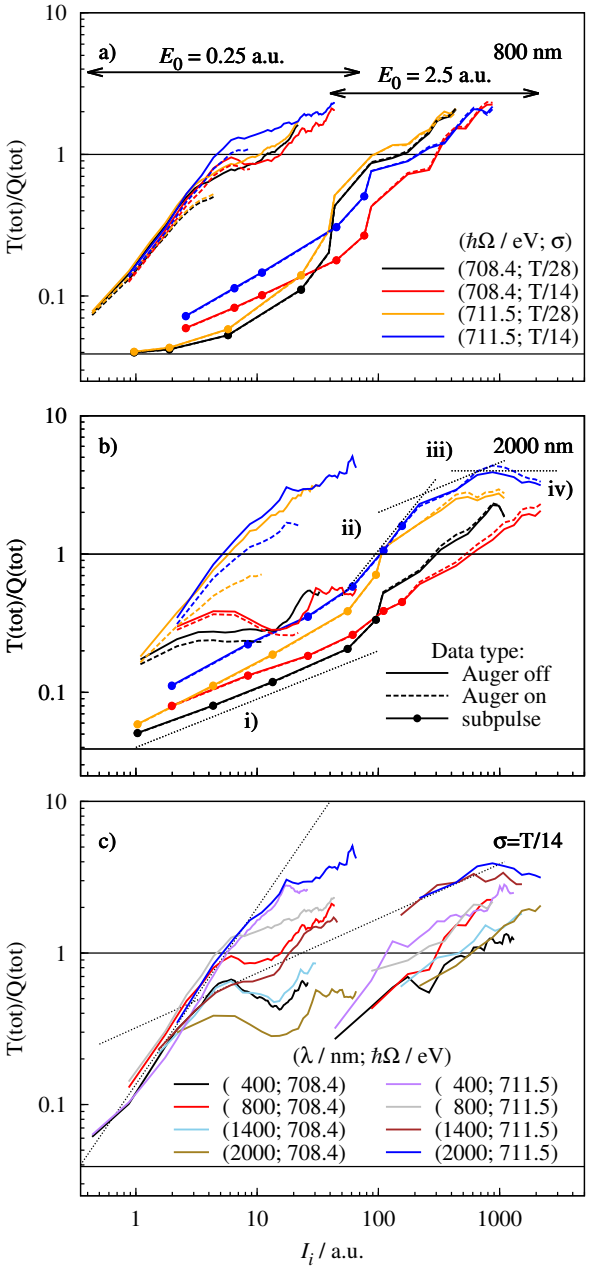

Figure III.5: Relative yield of the total triplet population to the total quintet one, T(tot)/Q(tot), versus the integrated intensity $I_i = \int_{-\infty}^{(t_{i+1}-t_i)/2} |\tilde{E}(t)|^2 dt$. The time $(t_{i+1} - t_i)/2$ corresponds to end of the ith subpulse in a train before $(i+1)$th subpulse starts. Two groups of branches with $E_0 = 0.25$ and 2.5 a.u. are observed. a) and b) correspond to the $\lambda = 800$ and 2000 nm. The population dynamics with/without Auger decay are shown as solid/dashed lines, respectively. To increase the overlap between the two branches, the first subpulse in a sequence with $E_0 = 2.5$ a.u. is subdivided; the respective data are shown with filled circles. c), the results for different λ are presented for $\sigma = T/14$. Two horizontal lines denote the starting T(tot)/Q(tot) and the point of T(tot)=Q(tot). Reprinted with permission from H. Wang, T. Möhle, O. Kühn, and S. I. Bokarev, Ultrafast dissipative spin-state dynamics triggered by x-ray pulse trains, Physical Review A, 98, 013408, (2018). Copyright 2018 by American Physical Society.

processes, thus, decreasing the rate of the spin crossover. The similar behavior of $E_0 = 0.25$ and 2.5 a.u. branches highlights that the pulse strength has only slight influence on the spin dynamics.

The pulse duration or the bandwidth of the pulse also have an influence on the dynamics, compare the cases with shorter duration $\sigma = T/28$ (panel d)) with the cases with longer one $\sigma = T/14$ (panel c)). Generally, the shorter one induces a faster oscillations which can be reasonably explained by the involvement of more distant states in the superposition for the larger bandwidth of the pulse. For the same E_0, the area under the $|\tilde{E}(t)|^2$ curve of the shorter pulse is smaller and thus they have weaker effect than the longer pulses. Interestingly, the delay between consecutive pulses also has moderate influence on the dynamics.

In summary, the ultrafast spin dynamics can also occur if triggered by pulse trains, and is similar to isolated pulse case. Multiple pulses lead to the stepwise pumping of triplet population which is more efficient. The characteristics of the subpulse in a train, such as carrier frequency, duration and delay are not influencing the dynamics of the system that much. However, the strength of the pulse causes a different behavior. The weak pulses are more selective and could be more suitable candidates to address ultrafast spin dynamics due to its better experimental availability. Still in experiment such electronic behavior can not be currently observed, because the intensity of the pulse generated from the HHG is only about $10^{12}\,\mathrm{W/cm^{-2}}$, which is much lower than the intensity used in our simulation for both strong and weak fields. In our case, even the intensity of the weak pulse reaches $10^{15}\,\mathrm{W/cm^{-2}}$. That is why, this problem represents a challenge for future experimental developments.

6 Energy Dissipation

In *regime V*, we accounted for the influence of the vibrational bath on the electron dynamics [**HW3**]. Thus, here we focus on the electron-vibrational coupling $\hat{H}_{\mathrm{S-B}}$ in Eq. II.1. Important to mention is that the electron-vibrational couplings are calculated by a quantum chemical hybrid approach on the basis of the shifted harmonic oscillators model. Here, the force constant matrix was determined at the level of DFT/B3LYP/6-311G(d) for the ground state and the gradients in the excited electronic states were computed at the ground state geometry using the RASSCF method as described in Section II. 3.

First, let us discuss the PESs along the most active tuning symmetric Fe-O breathing mode as shown in the panel b) of Fig. III.2. The result corresponds to PESs of core-excited electronic states in SOC basis, which are of main interest here. In this panel, a certain pattern with respect to the multiplicity of the states is apparent, which changes from quintet via strongly mixed to triplet with increasing energy. At the lower energy there are quintet states, then the quintet-triplet mixing dominates in the energy region 708-711 eV. An almost continuous density of states occur due to the splitting of the M_S-components, especially in energy region 708-711 eV which has been used for excitation in Section III. 4 and III. 5. From this Figure, we come to a conclusion that SOC is the dominant coupling mechanism if compared to the influence of electron-vibrational coupling. Thus this electron-vibrational coupling can be regarded as a small perturbation at short times. This justifies the Markov approximation used in our description of dissipation. Besides, the essentially continuous density of states justifies using simplified description by spectral density $J(\omega)$ instead of explicit wave packet propagation.

The spin dynamics of the selected valence and core SF and SOC states corresponding to the largest relaxation rates $k_{a\to b}$ are also shown in Fig. III.6 [**HW3**]. The envelope of the pulse with 132 as duration is shown with grey filled area, the solid and dash lines depict the case without and with bath, respectively. Panels a)-d) present the dynamics for core SF, valence SF, core SOC and valence SOC states. Valence SF states in panel b) show an oscillatory behavior which is typical for zero-order states building up a superposition in case of small coupling between them. In panel a) core SF states exhibit a more intricate pattern due to much stronger coupling and larger state density. In panels c) and d), without accounting for the dissipation, eigenstates of the SOC Hamiltonian stay stationary when the pulse is over. With vibrational bath, the

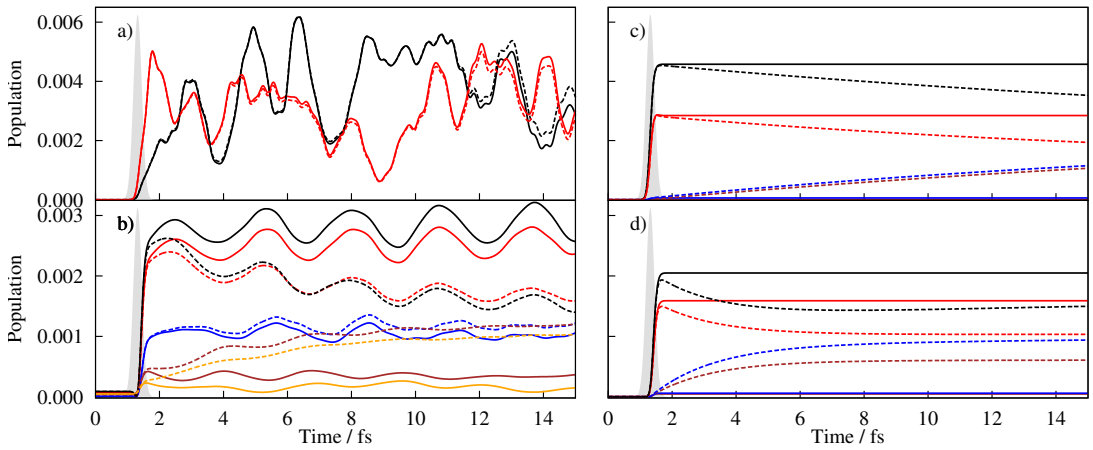

Figure III.6: *Regime V*, Population of selected states corresponding to the largest relaxation rates $k_{a\to b}$ with (dash lines) and without (solid lines) bath. a) core SF states; b) valence SF states; c) core SOC states; d) valence SOC states. The envelope of the excitation pulse is shown as a grey-shaded area.

population transfer between state pairs with largest relaxation rates $k_{a\to b}$ occurs. But the small amount of such pairs leads to the fact that such relaxation plays only a minor role within the time window of 15 fs. Although particular state populations with the largest $k_{a\to b}$ are notably affected by the dissipation as is illustrated in Fig. III.6, the populations of these states themselves are quite small what does not lead to notable differences in the dynamics of the total quintet and triplet populations shown in panel b) of Fig III.4. In this panel, the spin dynamics with and without bath are shown. Solid lines correspond to the case without bath and dash-dotted lines to the case considering the system-bath coupling. Comparing these two cases, the total quintet (red) and triplet (blue) populations are almost the same during the first 10 fs. Around 15 fs only slight differences can be seen. So one can conclude that the influence of the electron-vibrational coupling is very small, and can be ignored for the present dynamics.

In summary, the SOC driving force of the ultrafast spin flip is by far dominating over the effect of electron-vibrational coupling. Essentially, at least in the ultrashort time period which is considered in the work, the population relaxation due to vibrations can be neglected. More importantly, the dephasing caused by coupling to the nuclear bath is not destroying the coherence initially created by the absorption of the ultrashort pulse.

Chapter IV

Conclusions and Outlook

In this work, a new theoretical tool, density matrix-based time-dependent restricted active space configuration interaction (ρ-TD-RASCI), has been developed to study the many-electron dynamics. It has a number of advancements with respect to methods suggested before. This new method expands on the interplay between electron correlation and spin dynamics. SOC is calculated using atomic mean-field integral (AMFI) approximation and the electrons are restricted in an active space to describe the electronic core-excited states. For the study of the ultrafast spin dynamics in different regimes, one can use different basis states: CSF, SF and SOC to represent Hamiltonian and density matrix. The flexible choice of the basis makes the propagation for the simulation of the different processes convenient. CSF are used for electron correlation dynamics, SF basis is convenient to be used for spin dynamics and SOC states are used when dissipation needs to be accounted for.

The spin dynamics with different initial excitation conditions have been studied on the short time scale where the effect of the nuclear motion can be neglected. The spin dynamics considered here represents a new mechanism which is different from the conventional intersystem crossing. It is faster than usual SCO driven by nuclear motion and even faster than Auger decay. Such ultrafast spin dynamics should be typical for other core-hole states with nonzero angular momentum. Thus, the application of this effect can be extended to other TM systems.

To attain a better understanding of this phenomenon, we have studied different regimes. In *regime I*, the dynamics which is solely driven by strong electron correlation can be observed. This ultrafast process is analogous to CM, and relevant for core hole dynamics [169]. The timescales of such dynamics is faster than the core-hole migration observed in the ionized systems [106]. In the *regime II*, the ultrafast spin-flip dynamics solely driven by SOC is observed, which has been studied for easier understanding of the underlying mechanism. Here, the superposition of the strong spin-mixed core-hole states is instantaneously prepared, which is not stationary and evolves in time. Such process can be regarded as an elementary step of the conventional SCO driven by nuclear dynamics, similar to CM which is an elementary step of charge transfer driven by the nuclear motion. There is no doubt that the electronic wave packet dynamics will finally couple to nuclear motions, and after evolving for long enough time, finally charge or spin localisation will take place.

The *regime III* and *regime IV* demonstrate that the spin dynamics can be triggered by isolated soft X-ray light pulses as well as X-ray pulse trains. In these regimes, the effective

bandwidth is smaller than in *regime II*, but the ultrafast spin-flip still occurs. The timescale of such spin-flip dynamics is also faster than the lifetime of the $2p$ core hole. Importantly, the dynamics is sensitive to characteristics of the pulses such as carrier frequency, pulse duration, and amplitude. This enables to control the actual spin mixture to quite some extent with modest changes in the pulse. With the multiple pulses the stepwise population pumping occurs, and it seems that the characteristics of the individual pulse have less influence of the dynamics, while the strength of pulse plays an important role. Besides, valence excited states gain a substantial population for strong field which may attributed to stimulated emission. The weaker pulses are more selective in triggering spin dynamics. These two regimes are closer to the practical applications and could be more relevant to address or steer the ultrafast spin dynamics experimentally.

The last *regime V*, which is accounting for the influence of the bath demonstrates that the electron-vibrational coupling is small and its effect can be ignored at least at the short timescales below 50 fs. But we expect that its effect might be important and dominant for the processes, which are comparable or longer than the typical period of vibrations.

These regimes studied here theoretically, call for an experimental verification. However, the practical protocol to trigger spin dynamics by X-ray pulses until now is challenging. For the XFELs, the shortest duration for the soft X-ray pulse reached sub-10 fs [170] which is still too long to trigger the spin flip studied here. For HHG, the most challenging is the intensity of the generated pulse trains. Especially this applies to the isolated ultrafast pulses which needed some complicated additional techniques to be generated [57]. To the best of my knowledge, the intensity of the HHG pulses can only reach the magnitude of $10^{12}\,\mathrm{W/cm^{-2}}$, which is much lower than the intensity used in our simulations for both strong and weak fields (10^{15}-$10^{16}\,\mathrm{W/cm^{-2}}$). We expect that in future such application should be within reach.

The technique or method for practical initiation and measurement of such spin dynamics is also a challenge worth being considered. The upcoming time-resolved nonlinear X-ray spectroscopy, such as–stimulated resonant inelastic X-ray scattering (SRIXS) technique [171, 172, 173], could be considered as a possible direct way to realise such measurement. Within this technique, the mixed-spin core states can be projected onto the manifold of pure-spin valence states, which are usually energetically well separated in transition metal complexes [161, 162]. Thus, the relative SRIXS intensities in the respective energy ranges (0-1.5 eV for quintets and 1.5-8.2 eV for triplets in the case of $[Fe(H_2O)_6]^{2+}$system) would provide information on the time-evolution of the contribution of pure spin states to a mixed one. Another method is circular dichroism PES [174, 175, 176]. One can use the differential absorption of left and right circularly polarised light in a magnetic field to examine magnetic materials and properties. This technique has a major impact on the understanding of the physics of 3d transition metal, lanthanide and actinide systems and can be used to measure the behavior of bulk materials, magnetic nanostructures and clusters, and spin transport systems. With the rapid development of the HHG and XFELs, and the expected establishment of time-resolved techniques such as SRIXS, the experimental proof of the effect discussed here and its use for manipulating spin dynamics appears to be within reach.

This work represent a fundamental study to addressing the ultimate timescale of electron

dynamics caused by spin-orbit coupling. We envisage that this effect could be used for clocking ultrafast events. In this respect, it is of core-hole clock type [177] but has a different nature. Moreover, in case of spin-flips the characteristic timescale may be varied by addressing different atoms in the system or various types of core holes as well as by varying pulse characteristics, thus adjusting the strength of the coupling and thereby determining essentially the measured time window.

References

[1] N. M. Hugenholtz, "Quantum theory of many-body systems," *Rep. Prog. Phys.*, vol. 28, p. 201, 1965.

[2] E. S. Kryachko and E. V. Ludeña, *Energy Density Functional Theory of Many-Electron Systems*. Understanding Chemical Reactivity, Springer Netherlands, 1990.

[3] F. E. Harris, H. K. Monkhorst, and D. L. Freeman, *Algebraic and Diagrammatic Methods in Many-Fermion Theory*. New York: Oxford University Press Inc, 1992.

[4] J. C. Tremblay, T. Klamroth, and P. Saalfrank, "Time-dependent configuration-interaction calculations of laser-driven dynamics in presence of dissipation," *J. Chem. Phys.*, vol. 129, p. 084302, 2008.

[5] N. F. Scherer, J. L. Knee, D. D. Smith, and A. H. Zewail, "Laser femtochemistry," *J. Phys. Chem.*, vol. 89, pp. 5141–5143, 1985.

[6] H. Sakai, S. Minemoto, H. Nanjo, H. Tanji, and T. Suzuki, "Controlling the Orientation of Polar Molecules with Combined Electrostatic and Pulsed, Nonresonant Laser Fields," *Phys. Rev. Lett.*, vol. 90, 2003.

[7] D. Daems, S. Guérin, E. Hertz, H. R. Jauslin, B. Lavorel, and O. Faucher, "Field-Free Two-Direction Alignment Alternation of Linear Molecules by Elliptic Laser Pulses," *Phys. Rev. Lett.*, vol. 95, 2005.

[8] D. E. Spence, P. N. Kean, and W. Sibbett, "60-fsec pulse generation from a self-mode-locked ti:sapphire laser," *Opt. Lett.*, vol. 16, pp. 42–44, 1991.

[9] A. H. Zewail, "Laser femtochemistry," *Science*, vol. 242, pp. 1645–1653, 1988.

[10] A. H. Zewail, "Femtochemistry: Atomic-scale dynamics of the chemical bond," *J. Phys. Chem. A*, vol. 104, pp. 5660–5694, 2000.

[11] Y. Bhattacharjee, "Measuring the immeasurable," *Nature*, vol. 412, pp. 474–476, 2001.

[12] M. Dantus, M. J. Rosker, and A. H. Zewail, "Real time femtosecond probing of "transition states" in chemical reaction," *J. Chem. Phys.*, vol. 87, pp. 2395–2397, 1987.

[13] R. E.Walkup, J. A. Misewich, J. H. Glownia, and P. P. Sorokin, "Time-resolved absorption spectra of dissociating molecules," *Phys. Rev. Lett.*, vol. 65, pp. 2366–2369, 1990.

[14] S. K. Kim and A. H. Zewail, "Femtosecond elementary dynamics of transition states and asymmetric α-cleavage in norrish reactions," *Chem. Phys. Lett.*, vol. 250, pp. 279–286, 1996.

[15] M. Dantus, R. M. Bowman, M. Gruebele, and A. H. Zewail, "Femtosecond real?time probing of reactions. v. the reaction of ihgi," *J. Chem. Phys.*, vol. 91, pp. 7437–7450, 1989.

[16] T. S. Rose, M. J. Rosker, and A. H. Zewail, "Femtosecond real time probing of reactions. iv. the reactions of alkali halides," *J. Chem. Phys.*, vol. 91, pp. 7415–7436, 1989.

[17] R. R. Cavanagh, D. S. King, J. C. Stephenson, and T. F. Heinz, "Dynamics of nonthermal reactions: Femtosecond surface chemistry," *J. Phys. Chem.*, vol. 97, pp. 786–798, 1993.

[18] D. N. Denzler, C. Frischkorn, C. Hess, M. Wolf, and G. Ertl, "Electronic excitation and dynamic promotion of a surface reaction," *Phys. Rev. Lett.*, vol. 91, p. 226102, 2003.

[19] D. N. Denzler, C. Frischkorn, M. Wolf, and G. Ertl, "Surface femtochemistry: Associative desorption of hydrogen from ru(001) induced by electronic excitations," *J. Phys. Chem.*, vol. 250, pp. 14503–14510, 2004.

[20] A. Vierheilig, T. Chen, P. Waltner, W. Kiefer, A. Materny, and A. Zewail, "Femtosecond dynamics of ground-state vibrational motion and energy flow: Polymers of diacetylene," *Chem. Phys. Lett.*, vol. 312, pp. 349–356, 1999.

[21] T.-Q. Nguyen, J. Wu, V. Doan, B. J. Schwartz, and S. H. Tolber, "Control of energy transfer in oriented conjugated polymer-mesoporous silica composites," *Science*, vol. 288, pp. 652–656, 2000.

[22] H. J. Freund, "Model systems in heterogeneous catalysis: Selectivity studies at the atomic level," *Top Catal*, vol. 48, pp. 137–144, 2008.

[23] R. Rioux, *Model Systems in Catalysis: Single Crystals to Supported Enzyme Mimics*. New York, NY: Springer New York, 2010.

[24] X.-P. Li, O. Björkman, C. Shih, A. R. Grossman, M. Rosenquist, S. Jansson, and K. K. Niyogi, "A pigment-binding protein essential for regulation of pho tosynthetic light harvesting," *Science*, vol. 403, pp. 391–395, 2000.

[25] J.-M. L. Pecourt, J. Peon, and B. Kohler, "Ultrafast internal conversion of electronically excited rna and dna nucleosides in water," *J. Am. Chem. Soc.*, vol. 122, pp. 9348–9349, 2000.

[26] B. Schenkel, J. Biegert, U. Keller, C. Vozzia, M. Nisoli, G. Sansone, S. Stagira, S. D. Silvestri, and O. Svelto, "Generation of 38-fs pulses from adaptive compression of a cascaded hollow fiber supercontinuum," *Opt. Lett.*, vol. 28, pp. 1987–1989, 2003.

[27] G. Steinmeyer and G. Stibenz, "Generation of sub-4-fs pulses via compression of a white-light continuum using only chirped mirrors," *Appl. Phys. B*, vol. 82, pp. 175–181, 2006.

[28] A. E. Kaplan, "Subfemtosecond pulses in mode-locked 2π solitons of the cascade stimulated raman scattering," *Phys. Rev. Lett.*, vol. 73, pp. 1243–1246, 1994.

[29] S. E. Harris and A. V. Sokolov, "Subfemtosecond pulses generation by molecular modulation," *Phys. Rev. Lett.*, vol. 81, pp. 2894–2897, 1998.

[30] N. M. Naumova, J. A. Nees, I. V. Sokolov, B. Hou, and G. A. Mourou, "Relativistic generation of isolated attosecond pulses in a λ^3 focal volume," *Phys. Rev. Lett.*, vol. 92, p. 063902, 2004.

[31] J. Nees, N. Naumova, E. Power, V. Yanovsky, I. Sokolov, A. Maksimchuk, S.-W. Bahk, V. Chvykov, G. Kalintchenko, B. Hou, and G. Mourou, "Relativistic generation of isolated attosecond pulses: A different route to extreme intensity," *J. Modern Optics*, vol. 52, pp. 305–319, 2005.

[32] A. A. Zholents and W. M. Fawley, "Proposal for intense attosecond radiation from an x-ray free-electron laser," *Phys. Rev. Lett.*, vol. 92, p. 224801, 2004.

[33] A. A. Zholents and M. S. Zolotorev, "Attosecond x-ray pulses produced by ultra short transverse slicing via laser electron beam interaction," *New J. Phys.*, vol. 10, p. 25005, 2008.

[34] M. Hentschel, R. Kienberger, C. Spielmann, G. A. Reider, N. Milosevic, T. Brabec, P. Corkum, U. Heinzmann, M. Drescher, and F. Krausz, "Attosecond metrology," *Nature*, vol. 414, p. 509, 2001.

[35] S. Baker, I. A. Walmsley, J. W. G. Tisch, and J. P. Marangos, "Femtosecond to attosecond light pulses from a molecular modulator," *Nat. Photon.*, vol. 5, pp. 664–671, 2011.

[36] B. W. J. McNeil and N. R. Thompson, "X-ray free-electron lasers," *Nat. Photonics.*, vol. 4, pp. 814–821, 2010.

[37] G. Margaritondo and P. Rebernik Ribic, "A simplified description of X-ray free-electron lasers," *J. Synchrotron Radiation*, vol. 18, pp. 101–108, 2011.

[38] C. Pellegrini and J. Stöhr, "X-ray free-electron lasers—principles, properties and applications," *Nucl. Instrum. Methods Phys. Res. A*, vol. 500, pp. 33–40, 2003.

[39] E. Saldin, E. Schneidmiller, and M. Yurkov, "Self-amplified spontaneous emission fel with energ-chirped electron beam and its application for generation of attosecond x-ray pulses," *Phys. Rev. ST Accel. Beams*, vol. 9, p. 050702, 2006.

[40] J. D. Sadler, R. Nathvani, P. Oleśkiewicz, L. A. Ceurvorst, N. Ratan, M. F. Kasim, R. M. G. M. Trines, R. Bingham, and P. A. Norreys, "Compression of X-ray Free Electron Laser Pulses to Attosecond Duration," *Sci. Rep.*, vol. 5, p. 16755, 2015.

[41] S. Huang, Y. Ding, Z. Huang, and G. Marcus, "Generation of subterawatt-attosecond pulses in a soft x-ray free-electron laser," *Phys. Rev. ST Accel. Beams*, vol. 19, p. 080702, 2016.

[42] S. Serkez, G. Geloni, S. Tomin, G. Feng, E. V. Gryzlova, A. N. Grum-Grzhimailo, and M. Meyer, "Overview of options for generating high-brightness attosecond x-ray pulses at free-electron lasers and applications at the european xfel," *J. Opt.*, vol. 20, p. 024005, 2018.

[43] N. Hartmann, G. Hartmann, R. Heider, M. S. Wagner, M. Ilchen, J. Buck, A. O. Lindahl, C. Benko, J. Grünert, J. Krzywinski, J. Liu, A. A. Lutman, A. Marinelli, T. Maxwell, A. A. Miahnahri, S. P. Moeller, M. Planas, J. Robinson, A. K. Kazansky, N. M. Kabachnik, J. Viefhaus, T. Feurer, R. Kienberger, R. N. Coffee, and W. Helml, "Attosecond time-energy structure of X-ray free-electron laser pulses," *Nat. Photon.*, vol. 12, pp. 215–220, 2018.

[44] G. Edwards, R. Logan, M. Copeland, L. Reinisch, J. Davidson, B. Johnson, R. Maciunas, M. Mendenhall, R. Ossoff, J. Tribble, J. Werkhaven, and D. O'Day, "Tissue ablation by a free-electron laser tuned to the amide II band," *Nature*, vol. 371, pp. 416–419, 1994.

[45] M. Frank, D. B. Carlson, M. S. Hunter, G. J. Williams, M. Messerschmidt, N. A. Zatsepin, A. Barty, W. H. Benner, K. Chu, A. T. Graf, S. P. Hau-Riege, R. A. Kirian, C. Padeste, T. Pardini, B. Pedrini, B. Segelke, M. M. Seibert, J. C. H. Spence, C.-J. Tsai, S. M. Lane, X.-D. Li, G. Schertler, S. Boutet, M. Coleman, and J. E. Evans, "Femtosecond X-ray diffraction from two-dimensional protein crystals," *IUCrJ*, vol. 1, pp. 95–100, 2014.

[46] N. Bloembergen, *Nonlinear Optics*. Addison-Wesley Publishing Company, 1991.

[47] P. B. Corkum, "Plasma perspective on strong field multiphoton ionization," *Phys. Rev. Lett.*, vol. 71, pp. 1994–1997, 1993.

[48] K. Chang, Q. Zhang, M. Chini, Y. Wu, X. Wang, and Z. Chang, "Tailoring a 67 attosecond pulse through advantageous phase-mismatch," *Opt. Lett.*, vol. 37, pp. 3891–3893, 2012.

[49] D. Popmintchev, C. Hernandez-Garcia, F. Dollar, C. Mancuso, J. A. Perez-Hernandez, M.-C. Chen, A. Hankla, X. Gao, B. Shim, A. L. Gaeta, M. Tarazkar, D. A. Romanov, R. J. Levis, J. A. Gaffney, M. Foord, S. B. Libby, A. Jaron-Becker, A. Becker, L. Plaja, M. M. Murnane, H. C. Kapteyn, and T. Popmintchev, "Ultraviolet surprise: Efficient soft x-ray high-harmonic generation in multiply ionized plasmas," *Science*, vol. 350, pp. 1225–1231, 2015.

[50] B. Shan and Z. Chang, "Dramatic extension of the high-order harmonic cutoff by using a long-wavelength driving field," *Phys. Rev. A*, vol. 65, p. 011804, 2001.

[51] P. Colosimo, G. Doumy, C. I. Blaga, J. Wheeler, C. Hauri, F. Catoire, J. Tate, R. Chirla, A. M. March, G. G. Paulus, H. G. Muller, P. Agostini, and L. F. Dimauro, "Scaling strong-field interactions towards the classical limit," *Nat. Phys.*, vol. 4, pp. 386–389, 2008.

[52] N. Ishii, K. Kaneshima, K. Kitano, T. Kanai, S. Watanabe, and J. Itatani, "Carrier-envelope phase-dependent high harmonic generation in the water window using few-cycle infrared pulses," *Nat. Commun.*, vol. 5, p. 3331, 2014.

[53] T. Popmintchev, M.-C. Chen, D. Popmintchev, P. Arpin, S. Brown, S. Alivsauskas, G. Andriukaitis, T. Balčiunas, O. D. Mücke, A. Pugzlys, A. Baltuška, B. Shim, S. E. Schrauth, A. Gaeta, C. Hernández-García, L. Plaja, A. Becker, A. Jaron-Becker, M. M. Murnane, and H. C. Kapteyn, "Bright coherent ultrahigh harmonics in the kev x-ray regime from mid-infrared femtosecond lasers," *Science*, vol. 336, pp. 1287–1291, 2012.

[54] F. Brizuela, C. M. Heyl, P. Rudawski, D. Kroon, L. Rading, J. M. Dahlström, J. Mauritsson, P. Johnsson, C. L. Arnold, and A. L'Huillier, "Efficient high-order harmonic generation boosted by below-threshold harmonics," *Sci. Rep.*, vol. 3, 2013.

[55] C. Jin, G. Wang, H. Wei, A.-T. Le, and C. D. Lin, "Waveforms for optimal sub-keV high-order harmonics with synthesized two- or three-colour laser fields," *Nat. Commun.*, vol. 5, 2014.

[56] T. Kroh, C. Jin, P. Krogen, P. D. Keathley, A.-L. Calendron, J. P. Siqueira, H. Liang, E. L. Falcão-Filho, C. D. Lin, F. X. Kärtner, and K.-H. Hong, "Enhanced high-harmonic generation up to the soft X-ray region driven by mid-infrared pulses mixed with their third harmonic," *Opt. Express*, vol. 26, p. 16955, 2018.

[57] F. Krausz and M. Ivanov, "Attosecond physics," *Rev. Mod. Phys.*, vol. 81, pp. 163–234, 2009.

[58] R. Kienberger, E. Goulielmakis, M. Uiberacker, A. Baltuska, V. Yakovlev, F. Bammer, A. Scrinzi, T. Westerwalbesloh, U. Kleineberg, U. Heinzmann, M. Drescher, and F. Krausz, "Atomic transient recorder," *Nature*, vol. 817, p. 427, 2004.

[59] H. Mashiko, S. Gilbertson, C. Li, S. D. Khan, M. M. Shakya, E. Moon, and Z. Chang, "Double optical gating of high-order harmonic generation with carrier-envelope phase stabilized lasers," *Phys. Rev. Lett.*, vol. 100, p. 103906, 2008.

[60] H. Mashiko, S. Gilbertson, C. Li, E. Moon, and Z. Chang, "Optimizing the photon flux of double optical gated high-order harmonic spectra," *Phys. Rev. A*, vol. 77, p. 063423, 2008.

[61] G. Sansone, E. Benedetti, F. Calegari, C. Vozzi, L. Avaldi, R. Flammini, L. Poletto, P. Villoresi, C. Altucci, R. Velotta, S. Stagira, S. D. Silvestri, and M. Nisoli, "Isolated single-cycle attosecond pulses," *Science*, vol. 314, p. 443, 2006.

[62] I. J. Sola, E. Mevel, L. Elouga, E. Constant, V. Strelkov, L. Poletto, P. Villoresi, E. Benedtti, J. P. Caumes, S.Stagira, C. Vozzi, G. Sansone, and M. Nisoli, "Controlling attosecond electron dynamics by phase-stabilized polarization gating," *Nat. Phys.*, vol. 2, pp. 319–322, 2006.

[63] M. J. Abel, T. Pfeifer, P. M. Nagel, W. Boutu, M. J. Bell, C. P. Steiner, D. M. Neumark, and S. R. Leone, "Isolated attosecond pulses from ionization gating of high-harmonic emission," *Chem. Phys.*, vol. 336, pp. 9–14, 2009.

[64] F. Ferrari, F. Calegari, M. Lucchini, C. Vozzi, S. Stagira, G. Sansone, and M. Nisoli, "High-energy isolated attosecond pulses generated by above-saturation few-cycle fields," *Nat. Photonics.*, vol. 4, pp. 875–879, 2010.

[65] H. Vincenti and F. Quéré, "Attosecond lighthouses: How to use spatiotemporally coupled light fields to generate isolated attosecond pulses," *Phys. Rev. Lett.*, vol. 108, p. 113904, 2012.

[66] M. Louisy, C. L. Arnold, M. Miranda, E. W. Larsen, S. N. Bengtsson, D. Kroon, M. Kotur, D. Guénot, L. Rading, P. Rudawski, F. Brizuela, F. Campi, B. Kim, A. Jarnac, A. Houard, J. Mauritsson, P. Johnsson, A. L'Huillier, and C. M. Heyl, "Gating attosecond pulses in a noncollinear geometry," *Optica*, vol. 2, pp. 563–566, 2015.

[67] J. Li, X. Ren, Y. Yin, K. Zhao, A. Chew, Y. Cheng, E. Cunningham, Y. Wang, S. Hu, Y. Wu, M. Chini, and Z. Chang, "53-attosecond x-ray pulses reach the carbon k-edge," *Nat. Comm.*, vol. 8, pp. 1–5, 2017.

[68] M. Liebel, C. Schnedermann, T. Wende, and P. Kukura, "Principles and Applications of Broadband Impulsive Vibrational Spectroscopy," *J. Phys. Chem. A*, vol. 119, pp. 9506–9517, 2015.

[69] J. Du, J. Harra, M. Virkki, J. M. Mäkelä, Y. Leng, M. Kauranen, and T. Kobayashi, "Surface-Enhanced Impulsive Coherent Vibrational Spectroscopy," *Sci. Rep.*, vol. 6, 2016.

[70] D. R. Dietze and R. A. Mathies, "Femtosecond Stimulated Raman Spectroscopy," *Chem. Phys. Chem.*, vol. 17, pp. 1224–1251, 2016.

[71] H. Kuramochi, S. Takeuchi, and T. Tahara, "Femtosecond time-resolved impulsive stimulated Raman spectroscopy using sub-7-fs pulses: Apparatus and applications," *Rev. Sci. Instrum.*, vol. 87, p. 043107, 2016.

[72] P. Tzallas, E. Skantzakis, L. A. A. Nikolopoulos, G. D. Tsakiris, , and D. Charalambidis, "Extreme-ultraviolet pump-probe studies of one-femtosecond-scale electron dynamics," *Nat. Phys.*, vol. 7, pp. 781–784, 2011.

[73] A. Picón, C. S. Lehmann, C. Bostedt, A. Rudenko, A. Marinelli, T. Osipov, D. Rolles, N. Berrah, C. Bomme, M. Bucher, G. Doumy, B. Erk, K. R. Ferguson, T. Gorkhover, P. J. Ho, E. P. Kanter, B. Krässig, J. Krzywinski, A. A. Lutman, A. M. March, D. Moonshiram, D. Ray, L. Young, S. T. Pratt, and S. H. Southworth, "Hetero-site-specific x-ray pump-probe spectroscopy for femtosecond intramolecular dynamics," *Nat. Commun.*, vol. 7, p. 11652, 2016.

[74] B. Dromey, M. Zepf, A. Gopal, K. Lancaster, M. S. Wei, K. Krushelnick, M. Tatarakis, N. Vakakis, S. Moustaizis, R. Kodama, M. Tampo, C. Stoeckl, R. Clarke, H. Habara, D. Neely, S. Karsch, and P. Norreys, "High harmonic generation in the relativistic limit," *Nat. Phys.*, vol. 2, pp. 456–459, 2006.

[75] P. Zhang and A. G. R. Thomas, "Enhancement of high-order harmonic generation in intense laser interactions with solid density plasma by multiple reflections and harmonic amplification," *Appl. Phys. Lett.*, vol. 106, p. 131102, 2015.

[76] S. M. Teichmann, F. Silva, S. L. Cousin, M. Hemmer, and J. Biegert, "0.5-keV Soft X-ray attosecond continua," *Nat. Commun.*, vol. 7, p. 11493, 2016.

[77] M. Y. Ivanov, R. Kienberger, A. Scrinzi, and D. M. Villeneuve, "Attosecond physics," *J. Phys. B, J. Phys. B: At. Mol. Opt. Phys.*, vol. 39, pp. R1–R37, 2006.

[78] M. Drescher, M. Hentschel, R. Kienberger, M. Uiberacker, V. Yakovlev, A. Scrinzi, T. Westerwalbesloh, U. Kleineberg, U. Heinzmann, and F. Krausz, "Time-resolved atomic inner-shell spectroscopy," *Nature*, vol. 419, pp. 803–807, 2002.

[79] M. Drescher, M. Hentschel, R. Kienberger, M. Uiberacker, T. Westerwalbesloh, U. Kleineberg, U. Heinzmann, and F. Krausz, "Time-resolved atomic inner-shell spectroscopy," *J. Electron Spectrosc.*, vol. 137-140, pp. 259–264, 2004.

[80] G. Sansone, T. Pfeifer, K. Simeonidis, and A. I. Kuleff, "Electron correlation in real time," *Chem. Phys. Phys. Chem.*, vol. 13, pp. 661–680, 2012.

[81] A. Hauser, "Light-induced spin crossover and the high-spin $\rightarrow$ low-spin relaxation," *Top. Curr. Chem.*, vol. 234, pp. 155–198, 2004.

[82] C. Bressler, C. Milne, V.-T. Pham, A. E. R. M. van der Veen, W. Gawelda, S. Johnson, P. Beaud, D. Grolimund, M. Kaiser, C. N. Borca, G. Ingold, R. Abela, and M. Chergui, "Femtosecond xanes study of the light-induced spin crossover dynamics in an iron(ii) complex," *Science*, vol. 323, pp. 489–492, 2009.

[83] N. Huse, H. Cho, K. Hong, L. Jamula, F. M. F. de Groot, T. K. Kim, J. K. McCusker, and R. W. Schoenlein, "Femtosecond soft x-ray spectroscopy of solvated transition-metal complexes: Deciphering the interplay of electronic and structural dynamics," *J. Phys. Chem. Lett.*, vol. 2, pp. 880–884, 2011.

[84] D. Healion, Y. Zhang, J. D. Biggs, N. Govind, and S. Mukamel, "Entangled valence electron-hole dynamics revealed by stimulated attosecond x-ray raman scattering," *J. Phys. Chem. Lett.*, vol. 3, pp. 2326–2331, 2012.

[85] M. F. Kling and M. J. J. Vrakking, "Attosecond electron dynamics," *Annu. Rev. Phys. Chem.*, vol. 59, pp. 463–492, 2008.

[86] F. Krausz and M. Ivanov, "Attosecond physics," *Rev. Mod. Phys.*, vol. 81, pp. 163–234, 2009.

[87] F. Lépine, G. Sansone, and M. J. Vrakking, "Molecular applications of attosecond laser pulses," *Chem. Phys. Lett.*, vol. 1, p. 578, 2013.

[88] S. L. Chin, P. Agostini, and G. Ferrante, *Progress in Ultrafast Intense Laser Science III*. Springer Science & Business Media, Jan. 2008.

[89] L. X. Chen, X. Zhang, E. C. Wasinger, K. Attenkofer, G. Jennings, A. Z. Muresan, and J. S. Lindsey, "Tracking electrons and atoms in a photoexcited metalloporphyrin by x-ray transient absorption spectroscopy," *J. Am. Chem. Soc.*, vol. 129, pp. 9616–9618, 2007.

[90] M. L. Shelby, P. J. Lestrange, N. E. Jackson, K. Haldrup, M. W. Mara, A. B. Stickrath, D. Zhu, H. T. Lemke, M. Chollet, B. M. Hoffman, X. Li, and L. X. Chen, "Ultrafast excited state relaxation of a metalloporphyrin revealed by femtosecond x-ray absorption spectroscopy," *J. Am. Chem. Soc.*, vol. 138, pp. 8752–8764, 2016.

[91] A. R. J., M. Woerner, M. J. J. Vrakking, T. Elsaesser, E. L. Shirley, and A. Borgschulte, "Ultrafast modulation of electronic structure by coherent phonon excitations," *Phys. Rev. B*, vol. 95, p. 081101, 2017.

[92] E. Seres, J. Seres, and C. Spielmann, "X-ray absorption spectroscopy in the kev range with laser generated high harmonic radiation," *Appl. Phys. Lett.*, vol. 89, p. 181919, 2006.

[93] S. Mathias, C. La-O-Vorakiat, P. Grychtol, P. Granitzka, E. Turgut, J. M. Shaw, R. Adam, H. T. Nembach, M. E. Siemens, S. Eich, C. M. Schneider, T. J. Silva, M. Aeschlimann, M. M. Murnane, and H. C. Kapteyn, "Probing the timescale of the exchange interaction in a ferromagnetic alloy," *Proc. Natl. Acad. Sci. U.S.A.*, vol. 109, p. 4792, 2012.

[94] A. D. Dutoi, M. Wormit, and L. S. Cederbaum, "Ultrafast charge separation driven by differential particle and hole mobilities.," *J. Chem. Phys.*, vol. 134, p. 24303, 2011.

[95] A. D. Dutoi and L. S. Cederbaum., "An excited electron avoiding a positive charge.," *J. Phys. Chem. Lett.*, vol. 2, pp. 2300–2303, 2011.

[96] H. M. Jaeger and O. V. Prezhdo, "Exciton dynamics: Electrons take an unexpected turn.," *Nat. Chem.*, vol. 4, pp. 8–10, 2011.

[97] I. V. Schweigert and S. Mukamel, "Probing valence electronic wave-packet dynamics by all x-ray stimulated Raman spectroscopy: A simulation study," *Phys. Rev. A*, vol. 76, 2007.

[98] S. Lünnemann, A. I. Kuleff, and L. S. Cederbaum, "Ultrafast electron dynamics following outer-valence ionization: The impact of low-lying relaxation satellite states," *J. Chem. Phys.*, vol. 130, p. 154305, 2009.

[99] A. I. Kuleff, S. Lünnemann, and L. S. Cederbaum, "Electron-correlation-driven charge migration in oligopeptides," *Chem. Phys.*, vol. 414, pp. 100–105, 2013.

[100] A. I. Kuleff, J. Breidbach, and L. S. Cederbaum, "Multielectron wave-packet propagation: General theory and application," *J. Chem. Phys.*, vol. 123, p. 044111, 2005.

[101] J. Breidbach and L. S. Cederbaum, "Migration of holes: Formalism, mechanisms, and illustrative applications," *J. Chem. Phys.*, vol. 118, pp. 3983–3996, 2003.

[102] L. S. Cederbaum and J. Zobeley, "Ultrafast charge migration by electron correlation," *Chem. Phys. Lett.*, vol. 307, pp. 205–210, 1999.

[103] H. Hennig, J. Breidbach, and L. S. Cederbaum, "Electron Correlation as the Driving Force for Charge Transfer: Charge Migration Following Ionization in N-Methyl Acetamide," *J. Phys. Chem. A*, vol. 109, pp. 409–414, 2005.

[104] F. Remacle and R. D. Levine, "An electronic time scale in chemistry," *Proc. Nat. Acad. Sci.*, vol. 103, pp. 6793–6798, 2006.

[105] A. I. Kuleff and L. S. Cederbaum, "Radiation generated by the ultrafast migration of a positive charge following the ionization of a molecular system," *Phys. Rev. Lett.*, vol. 106, p. 053001, 2011.

[106] A. I. Kuleff and L. S. Cederbaum, "Ultrafast correlation-driven electron dynamics," *J. Phys. B*, vol. 47, p. 124002, 2014.

[107] F. Calegari, D. Ayuso, A. Trabattoni, L. Belshaw, S. D. Camillis, S. Anumula, F. Frassetto, L. Poletto, A. Palacios, P. Decleva, J. B. Greenwood, F. Martín, and M. Nisoli, "Ultrafast electron dynamics in phenylalanine initiated by attosecond pulses," *Science*, vol. 346, pp. 336–339, 2014.

[108] P. M. Kraus, B. Mignolet, D. Baykusheva, A. Rupenyan, L. Horny, E. F. Penka, G. Grassi, O. I. Tolstikhin, J. Schneider, F. Jensen, L. B. Madsen, A. D. Bandrauk, F. Remacle, and H. J. Worner, "Measurement and laser control of attosecond charge migration in ionized iodoacetylene," *Science*, vol. 350, pp. 790–795, 2015.

[109] W. von Niessen and L. S. Cederbaum, "Many-body calculations on the ionization spectra of transition metal compounds: $Zncl_2$, $cdcl_2$ and $nicl_2$," *Mol. Phys.*, vol. 43, pp. 897–911, 1981.

[110] M. S. Deleuze, M. G. Giuffreda, and J.-P. François, "Valence one-electron and shake-up ionization bands of carbon clusters. ii. the c_n (n=4,6,8,10) rings," *J. Chem. Phys.*, vol. 112, p. 5325, 2000.

[111] M. Ehara, M. Nakata, and H. Nakatsuji, "Valence ionization spectra of 4π-electron molecules with low-lying satellites involving n-π^* and $\pi - \pi^*$ transitions," *Mol. Phys.*, vol. 104, pp. 971–982, 2006.

[112] T. Okino, K. Yamanouchi, T. Shimizu, K. Furusawa, H. Hasegawa, Y. Nabekawa, and K. Midorikawa, "Attosecond molecular coulomb explosion," *Chem. Phys. Lett.*, vol. 432, pp. 68–73, 2006.

[113] G. Sansone, F. Kelkensberg, J. F. Pérez-Torres, F. Morales, M. F. Kling, W. Siu, O. Ghafur, P. Johnsson, M. Swoboda, E. Benedetti, F. Ferrari, F. Lépine, J. L. Sanz-Vicario, S. Zherebtsov, I. Znakovskaya, A. L'Huillier, M. Y. Ivanov, M. Nisoli, F. Marín, and M. J. J. Vrakking, "Electron localization following attosecond molecular photoionization," *Nature*, vol. 465, pp. 763–767, 2010.

[114] F. Kelkensberg, W. Siu, J. F. Pérez-Torres, F. Morales, G. Gademann, A. Rouzée, P. Johnsson, M. Lucchini, F. Calegari, J. L. Sanz-Vicario, F. Martín, and M. J. J. Vrakking,

"Attosecond control in photoionization of hydrogen molecules," *Phys. Rev. Lett.*, vol. 107, p. 043002, 2011.

[115] A. D. Dutoi, K. Gokhberg, and L. S. Cederbaum, "Time-resolved pump-probe spectroscopy to follow valence electronic motion in molecules: Theory.," *Phys. Rev. A*, vol. 88, p. 013419, 2013.

[116] D. Healion, Y. Zhang, J. D. Biggs, N. Govind, and S. Mukamel, "Entangled valence electron-hole dynamics revealed by stimulated attosecond x-ray raman scattering," *J. Phys. Chem. Lett.*, vol. 3, pp. 2326–2331, 2012.

[117] G. Hermann and J. C. Tremblay, "Laser-Driven Hole Trapping in a Ge/Si Core–Shell Nanocrystal: An Atomistic Configuration Interaction Perspective," *J. Phys. Chem. C*, vol. 119, pp. 25606–25614, 2015.

[118] J. C. Tremblay, S. Klinkusch, T. Klamroth, and P. Saalfrank, "Dissipative many-electron dynamics of ionizing systems," *J. Chem. Phys.*, vol. 134, p. 044311, 2011.

[119] A. D. Dutoi, "Visualising many-body electron dynamics using one-body densities and orbitals," *Mol. Phys.*, vol. 112, pp. 1–11, 2014.

[120] J. Schirmer, "Beyond the random-phase approximation: A new approximation scheme for the polarization propagator," *Phys. Rev. A*, vol. 26, pp. 2395–2416, 1982.

[121] J. Schirmer, L. S. Cederbaum, and O. Walter, "New approach to the one-particle green's function for finite fermi systems," *Phys. Rev. A*, vol. 28, pp. 1237–1259, 1983.

[122] A. D. Dutoi, L. S. Cederbaum, M. Wormit, J. H. Starcke, and Andreas, "Tracing molecular electronic excitation dynamics in real time and space.," *J. Chem. Phys.*, vol. 132, p. 144302, 2010.

[123] Z. Li, O. Vendrell, and R. Santra, "Ultrafast charge transfer of a valence double hole in glycine driven exclusively by nuclear motion," *Phys. Rev. Lett.*, vol. 115, p. 143002, 2015.

[124] V. Despre, A. Marciniak, V. Loriot, M. C. E. Galbraith, A. Rouze e, M. J. J. Vrakking, Lépine, F., and A. I. Kuleff, "Attosecond Hole Migration in Benzene Molecules Surviving Nuclear Motion," *J. Phys. Chem. Lett.*, vol. 6, pp. 426–431, 2015.

[125] B. Cooper and V. Averbukh, "Single-Photon Laser-Enabled Auger Spectroscopy for Measuring Attosecond Electron-Hole Dynamics," *Phys. Rev. Lett.*, vol. 111, p. 083004, 2013.

[126] D. Mendive-Tapia, M. Vacher, M. J. Bearpark, and M. A. Robb, "Coupled electron-nuclear dynamics: Charge migration and charge transfer initiated near a conical intersection," *J. Chem. Phys.*, vol. 139, p. 044110, 2013.

[127] A. I. Kuleff and L. S. Cederbaum, "Charge migration in different conformers of glycine: The role of nuclear geometry," *Chem. Phys.*, vol. 338, pp. 320–328, 2007.

[128] M. Vacher, M. J. Bearpark, and M. A. Robb, "Communication: Oscillating charge migration between lone pairs persists without significant interaction with nuclear motion in the glycine and gly-gly-nh-ch$_3$ radical cations," *J. Chem. Phys.*, vol. 140, p. 201102, 2014.

[129] A. Dreuw, G. A. Worth, L. S. Cederbaum, and M. Head-Gordon, "Ultrafast photoinitiated long-range electron transfer in cyclophane-bridged zincporphyrin-quinone complexes via conical intersections," *J. Phys. Chem. B*, vol. 108, pp. 19049–19055, 2004.

[130] O. Tishchenko, R. Li, and D. G. Truhlar, "Metal-organic charge transfer can produce biradical states and is mediated by conical intersections," *Pro. Nat. Acad. Sci.*, vol. 107, pp. 19139–19145, 2010.

[131] B. Giese, S. Eckhardt, and M. Lauz, *Electron Transfer in Peptides and Proteins.* American Cancer Society, 2012.

[132] A. Cannizzo, C. Milne, C. Consani, W. Gawelda, C. Bressler, F. van Mourik, and M. Chergui, "Light-induced spin crossover in fe(ii)-based complexes: The full photocycle unraveled by ultrafast optical and x-ray spectroscopies," *Coord. Chem. Rev.*, vol. 254, pp. 2677–2686, 2010.

[133] C. Sousa, C. de Graaf, A. Rudavskyi, R. Broer, J. Tatchen, M. Etinski, and C. M. Marian, "Ultrafast deactivation mechanism of the excited singlet in the light-induced spin crossover of $[fe(2,2-bipyridine)_3]^{2+}$," *Chem. Eur. J.*, vol. 19, pp. 17541–17551, 2013.

[134] G. Auböck and M. Chergui, "Sub-50-fs photoinduced spin crossover in [fe(bpy)$_3$]$^{2+}$," *Nat. Chem.*, vol. 7, pp. 629–633, 2015.

[135] J. J. McGarvey, I. Lawthers, K. Heremans, and H. Toftlund, "Spin-state relaxation dynamics in iron(ii) complexes: solvent effects on the activation and reaction volumes for the $^1a \rightleftharpoons {}^5t$ interconversion.," *J. Chem. Soc. Chem. Commun.*, pp. 1575–1576, 1984.

[136] S.Decurtins, P. Gutlich, C. P. Kohler, and H. Spiering, "New examples of light-induced excited spin state trapping (liesst) in iron(ii) spin-crossover systems," *J. Chem. Soc. Chem. Commun.*, pp. 430–432, 1985.

[137] A. Gaspar, M. Seredyuk, and P. Gütlich, "Spin crossover in metallomesogens," *Coord. Chem. Rev.*, vol. 253, pp. 2399–2413, 2009.

[138] M. A. Halcrow, *Spin-Crossover Materials: Properties and Applications.* John Wiley & Sons, 2013.

[139] T. Dietl, D. Awschalom, M. Kaminska, and H. Ohno, *Spintronics in Semiconductors and Semimetals.* Amsterdam: Academic Press, 2008.

[140] S. D. Bader and S. Parkin, "Spintronics," *An. Rev. Cond. Matt. Phys.*, vol. 1, pp. 71–88, 2010.

[141] A. Bhattacharjee, P. J. van Koningsbruggen, W. Hibbs, J. S. Miller, and P. Gütlich, "Study of thermal spin crossover in [fe(ii)(isoxazole)$_6$]$(bf_4)_2$ with mössbauer spectroscopy," *J. Phys: Condens. Matter*, vol. 19, p. 406202, 2007.

[142] M. Nihei, T. Shiga, Y. Maeda, and H. Oshio, "Spin crossover iron(III) complexes," *Coord. Chem. Rev.*, vol. 251, pp. 2606–2621, 2007.

[143] J. E. Monat and J. K. McCusker, "Femtosecond excited-state dynamics of an iron(ii) polypyridyl solar cell sensitizer model," *J. Am. Chem. Soc.*, vol. 122, pp. 4092–4297, 2000.

[144] A. L. Smeigh, M. Creelman, R. A. Mathies, and J. K. McCusker, "Femtosecond time-resolved optical and raman spectroscopy of photoinduced spin crossover: Temporal resolution of low-to-high spin optical switching," *J. Am. Chem. Soc.*, vol. 130, pp. 14105–14107, 2008.

[145] K. Atak, R. Golnak, J. Xiao, E. Suljoti, M. Pflüger, T. Brandenburg, B. Winter, and E. F. Aziz, "Electronic Structure of Hemin in Solution Studied by Resonant X-ray Emission Spectroscopy and Electronic Structure Calculations," *J. Phys. Chem. B*, vol. 118, pp. 9938–9943, 2014.

[146] J. C. Tremblay, P. Krause, T. Klamroth, and P. Saalfrank, "Time-dependent response of dissipative electron systems," *Phys. Rev. A*, vol. 81, 2010.

[147] V. May and O. Kühn, *Charge and Energy Transfer Dynamics in Molecular Systems*. Weinheim : Wiley-VCH, 3., rev. and enl. ed. ed., 2011.

[148] P.-A. Malmqvist, A. Rendell, and B. O. Roos, "The restricted active space self-consistent-field method, implemented with a split graph unitary group approach," *J. Phys. Chem.*, vol. 94, pp. 5477–5482, 1990.

[149] B. A. Heß, C. M. Marian, U. Wahlgren, and O. Gropen, "A mean-field spin-orbit method applicable to correlated wavefunctions," *Chem. Phys. Lett.*, vol. 251, pp. 365–371, 1996.

[150] B. O. Roos, P. R. Taylor, and P. Siegbahn, "A complete active space SCF method (CASSCF) using a density matrix formulated super-CI approach," *Chem. Phys.*, vol. 48, pp. 157–173, 1980.

[151] J. Olsen, B. O. Roos, P. Jørgensen, and H. J. A. Jensen, "Determinant based configuration interaction algorithms for complete and restricted configuration interaction spaces," *J. Chem. Phys.*, vol. 89, p. 2185, 1988.

[152] P. A. Malmqvist, A. Rendell, and B. O. Roos, "The restricted active space self-consistent-field method, implemented with a split graph unitary group approach," *J. Phys. Chem.*, vol. 94, pp. 5477–5482, 1990.

[153] J. Hinze, "Mcscf. i. the multi-configuration self-consistent field method," *J. Chem. Phys.*, vol. 59, pp. 6424–6432, 1973.

[154] R. J. Gdanitz and R. Ahlrichs, "The averaged coupled-pair functional (ACPF): A size-extensive modification of MR CI(SD)," *Chem. Phys. Lett.*, vol. 143, pp. 413–420, 1988.

[155] W. Duch and G. H. F. Diercksen, "Size-extensivity corrections in configuration interaction methods," *J. Chem. Phys.*, vol. 101, pp. 3018–3030, 1994.

[156] O. Christiansen, J. Gauss, and B. Schimmelpfennig, "Spin-orbit coupling constants from coupled-cluster response theory," *Phys. Chem. Chem. Phys*, vol. 2, pp. 965–971, 2000.

[157] S. Mukamel, *Principles of nonlinear optical spectroscopy.* New York: Oxford Univ. Press, 1999.

[158] J. Stöhr, *NEXAFS Spectroscopy.* Berlin, New York: Springer-Verlag, 1992.

[159] M. Ohno, "An analysis of the coincidence l2-l3m4,5 coster-kronig preceded auger decay spectra of fe and co and the related auger-auger electron coincidence spectroscopy (AACS) spectra," *J. El. Spec. Rel. Phen.*, vol. 171, pp. 1–17, 2009.

[160] S. I. Bokarev, E. S. M. Dantz, O. Kühn, and E. F. Aziz, "State-dependent electron delocalization dynamics at the solute-solvent interface: Soft x-ray absorption spectroscopy and ab initio calculations," *Phys. Rev. Lett.*, vol. 111, p. 083002, 2013.

[161] S. I. Bokarev, M. Khan, M. K. Abdel-Latif, J. Xiao, R. Hilal, S. G. Aziz, E. F. Aziz, and O. Kühn, "Unraveling the Electronic Structure of Photocatalytic Manganese Complexes by L-Edge X-ray Spectroscopy," *J.Phys. Chem. C*, vol. 119, pp. 19192–19200, 2015.

[162] R. Golnak, S. I. Bokarev, R. Seidel, J. Xiao, G. Grell, K. Atak, I. Unger, S. Thürmer, S. G. Aziz, O. Kühn, B. Winter, and E. F. Aziz, "Joint analysis of radiative and non-radiative electronic relaxation upon x-ray irradiation of transition metal aqueous solutions," *Sci. Rep.*, vol. 6, p. 24659, 2016.

[163] K. Atak, S. I. Bokarev, R. G. M. Gotz, K. M. Lange, N. Engel, M. Dantz, E. Suljoti, O. Kühn, and E. F. Aziz, "The nature of the chemical bond of aqueous fe^{2+} probed by soft x-ray spectroscopies and ab initio calculations," *J. Phys. Chem. B*, vol. 117, pp. 12613–12618, 2013.

[164] M. Douglas and N. M. Kroll, "Quantum electrodynamical corrections to the fine structure of helium," *Ann. Phys.*, vol. 82, pp. 89–155, 1974.

[165] J. A. Gaj and J. Kossut, eds., *Introduction to the Physics of Diluted Magnetic Semiconductors*, vol. 144 of *Springer Series in Materials Science.* Berlin, Heidelberg: Springer Berlin Heidelberg, 2010.

[166] S. Mai, P. Marquetand, and L. González, "A general method to describe intersystem crossing dynamics in trajectory surface hopping," *Int. J. Quantum Chem.*, vol. 115, pp. 1215–1231, 2015.

[167] M. Bargheer, R. B. Gerber, M. V. Korolkov, O. Kühn, J. Manz, M. Schröder, and N. Schwentner, "Subpicosecond spin-flip induced by the photodissociation dynamics of clf in an ar matrix," *Phys. Chem. Chem. Phys.*, vol. 4, pp. 5554–5562, 2002.

[168] M. Hada and J. Matsuo, "Ultrafast X-ray sources for time-resolved measurements: Review of ultrafast X-ray sources," *X-Ray Spectrom.*, vol. 41, pp. 188–194, 2012.

[169] G. Hermann and J. C. Tremblay, "Laser-Driven Hole Trapping in a Ge/Si Core–Shell Nanocrystal: An Atomistic Configuration Interaction Perspective," *J. Phys. Chem. C*, vol. 119, pp. 25606–25614, 2015.

[170] C. Behrens, F.-J. Decker, Y. Ding, V. A. Dolgashev, J. Frisch, Z. Huang, P. Krejcik, H. Loos, A. Lutman, T. J. Maxwell, J. Turner, J. Wang, M.-H. Wang, J. Welch, and J. Wu, "Few-femtosecond time-resolved measurements of X-ray free-electron lasers," *Nat. Commun.*, vol. 5, 2014.

[171] S. Mukamel, D. Healion, Y. Zhang, and J. D. Biggs, "Multidimensional attosecond resonant x-ray spectroscopy of molecules: Lessons from the optical regime," *An. Rev. Phys. Chem.*, vol. 64, pp. 101–127, 2013.

[172] D. J. Haxton and C. W. McCurdy, "Ultrafast population transfer to excited valence levels of a molecule driven by x-ray pulses," *Phys. Rev. A*, vol. 90, p. 053426, 2014.

[173] Y. Zhang, W. Hua, K. Bennett, and S. Mukamel, "Nonlinear spectroscopy of core and valence excitations using short x-ray pulses: Simulation challenges," *Top. Curr. Chem.*, vol. 368, pp. 273–345, 2015.

[174] K. Nakanishi, N. Berova, and R. Woody, *Circular Dichroism: Principles and Applications*. VCH, 1994.

[175] R. Pagni, "Circular Dichroism and Linear Dichroism," *J. Chem. Educ.*, vol. 75, p. 1095, 1998.

[176] P. W. Atkins and J. De Paula, *Elements of physical chemistry*. Oxford ; New York: Oxford University Press, 5th ed ed., 2009.

[177] M. N. Piancastelli, G. Goldsztejn, T. Marchenko, R. Guillemin, R. K. Kushawaha, L. Journel, S. Carniato, J.-P. Rueff, D. Céolin, and M. Simon, "Core-hole-clock spectroscopies in the tender x-ray domain," *J. Phys. B: At. Mol. Opt. Phys.*, vol. 47, p. 124031, 2014.

Appendix A

Own Contributions to the Manuscripts

Peer Reviewed Publications

[**HW1**]: Huihui Wang, Sergey I. Bokarev, Saadullah G. Aziz, and Oliver Kühn, Ultrafast Spin-State Dynamics in Transition-Metal Complexes Triggered by Soft-X-Ray Light, *Physical Review Letters* **118**, 023001 (2017)

My contribution: I have developed a theoretical method leading to the numerical protocol that has been implemented by me. I have performed the numerical simulations and produced the presented figures. I have drafted the article after the results have been interpreted together with the coauthors. Subsequently, the text has been iterated to its final form by me and the coauthors.

[**HW2**]: Huihui Wang, Sergey I. Bokarev, Saadullah G. Aziz, and Oliver Kühn, Density matrix-based time-dependent configuration interaction approach to ultrafast spin-flip dynamics, *Molecular Physics* **115**, 1898-1907 (2017)

My contribution: Using the method developed in [**HW1**], I have performed all numerical simulations and produced the presented figures. I have interpreted the results, drafted the article and iterated the text to its final stage together with the coauthors.

[**HW3**]: Huihui Wang, Tobias Möhle, Oliver Kühn, and Sergey I. Bokarev, Ultrafast dissipative spin-state dynamics triggered by x-ray pulse trains, *Physical Review A* **98**, 013408 (2018)

My contribution: I have developed the employed theoretical expressions leading to the presented numerical protocol that has been implemented by me. I have performed the numerical simulations and produced the figures. Together with the coauthors, I have interpreted the results, drafted the article and iterated the text.

Appendix B

Peer Reviewed Publications

[HW1] Ultrafast Spin-State Dynamics in Transition-Metal Complexes Triggered by Soft-X-Ray Light

Huihui Wang, Sergey I. Bokarev, Saadullah G. Aziz, and Oliver Kühn

Physical Review Letters **118**, 023001 (2017)

Article DOI: https://doi.org/10.1103/PhysRevLett.118.023001
Erratum DOI: https://doi.org/10.1103/PhysRevLett.120.269901

[HW2] Density matrix-based time-dependent configuration interaction approach to ultrafast spin-flip dynamics

Huihui Wang, Sergey I. Bokarev, Saadullah G. Aziz, and Oliver Kühn

Molecular Physics **115**, 1898-1907 (2017)

Article DOI: https://doi.org/10.1080/00268976.2017.1294267
Corrigendum DOI: https://doi.org/10.1080/00268976.2018.1489539

[HW3] Ultrafast dissipative spin-state dynamics triggered by x-ray pulse trains

Huihui Wang, Tobias Möhle, Oliver Kühn, and Sergey I. Bokarev

Physical Review A **98**, 013408 (2018)

DOI: https://doi.org/10.1103/PhysRevA.98.013408

Aknowledgments

First of all, I would like to express my gratitude to Prof. Dr. Oliver Kühn, who enabled me to work scientifically during my doctoral studies in his research group Molecular Quantum Dynamics. His support not only through inspirational discussions and the constructive collaboration on the publications but also on the friendly atmosphere within the working group.

Special thanks to Dr. Sergey I. Bokarev, who help me with his useful and constructive advices and nice guidance throughout the whole work. He always encourage me with inspiring words and give me professional assistance in the theory, programming and scientific writing.

Thanks for the financial support by the Deanship of Scienctific Rearch (DSR), King Abdulaziz University, Jeddah (Grant No. D-003-435).

I am also indebted to my colleagues in our group AGQD, especially Dr. Olga Bokareva for her mental support when I first arrived in Rostock and great support in motivating me to learn and speak German language.

Finally, my heartfelt gratitude goes also to my parents and my brother who have always been helping me in case of difficulties and supporting without a word of complaint. I also owe my gratitude to my friends in Rostock and in my hometown who made my life easier and funnier during all the years of study.

Eidesstattliche Versicherung

Ich versichere hiermit an Eides statt, dass ich die vorliegende Arbeit selbstständig angefertigt und ohne fremde Hilfe verfasst habe. Dazu habe ich keine außer den von mir angegebenen Hilfsmitteln und Quellen verwendet und die den benutzten Werken inhaltlich und wörtlich entnommenen Stellen habe ich als solche kenntlich gemacht.

Rostock

(Abgabedatum)	(Vollständige Unterschrift)